

A complete determination of vibrational energy transfer pathways in CH₂D₂ for states below 3000 cm⁻¹: A laser induced fluorescence study

Mark Moser, V. A. Apkarian, and Eric Weitz^{a)}

Department of Chemistry and Materials Research Center, Northwestern University, Evanston, Illinois 60201
(Received 24 June 1980; accepted 11 September 1980)

Vibrational energy transfer processes in dideuteromethane were studied using a variety of complementary, laser induced fluorescence techniques. The time evolution of population in all infrared active fundamentals, except ν_4 and ν_7 , were monitored following three different initial conditions: excess population in ν_7 , excess population in a 2000 cm⁻¹ state, and simultaneous excess population in ν_4 and a 2000 cm⁻¹ state. These initial perturbations were achieved by irradiating the molecule with the *R*(22), *P*(24), and *P*(38) lines of the 9.6 μ CO₂ laser band. Experiments were performed on pure CH₂D₂, CH₂D₂ rare gas, and CH₂D₂-O₂ mixtures in order to elucidate the vibrational equilibration pathways in the parent molecule. The experimental studies afforded a complete map of the energy transfer pathways between the fundamentals and yielded rate constant for some specific *V-V* steps. The validity of these conclusions were confirmed by numerical modeling of the system. Theoretical calculations based on the Sharma and Brau, and Schwartz, Slawsky, and Herzfeld formulations were performed to conclude that *V-V* processes in CH₂D₂ are governed almost exclusively by hard core collisions.

I. INTRODUCTION

The general phenomenon of laser-induced fluorescence has been known for many years and has been used as a technique to obtain detailed information concerning vibration to vibration (*V-V*) and vibration to translation/rotation (*V-T/R*) energy transfer processes in polyatomic molecules. In recent years, many new variations of the technique have been developed in order to facilitate the assignment of vibrational energy transfer pathways and specific rate constants in complex molecular systems, thus making it possible to compare experimentally determined rate constants to those predicted theoretically in an effort to better understand the dynamics of these processes.¹

The investigations of CH₂D₂, reported on in this paper, provide an important link in the experimental and theoretical studies of vibrational energy transfer in the substituted methanes. The CH₂D₂ molecule is an extremely asymmetric top with nine nondegenerate vibrations. Despite the high density and complexity of structure common to asymmetric top molecules the spectroscopy of CH₂D₂ has been thoroughly studied.² Due to its C_{2v} symmetry, the molecule possesses a non IR active state, ν_5 , and contains dipole nonallowed *V-V* transitions. It was expected that this property would have a measurable effect on the vibrational equilibrium processes of the molecule.³ However, due to the small dipole moment derivatives associated with the vibrational transitions in CH₂D₂, its energy transfer processes are not governed (to any significant extent) by long-range electric multipolar interactions. Therefore, all such consequences of symmetry considerations appear to vanish. This point will be further expanded upon in Sec. IV D.

Recently, CH₂D₂ has been employed in studies of isotopically selective chemistry.⁴ Knowledge of path-

ways and rates of vibrational equilibration are relevant to such studies. Therefore, results in this paper should prove useful to further efforts in this direction.

CH₂D₂ proved itself amenable to a variety of diagnostic techniques that made the complete determination of the details of its vibrational equilibration processes possible. Of these techniques, one that is simplest conceptually, but seldom feasible, is the comparison of the time-dependent population response of a given mode when the initially excited state is varied. The infrequent application of this technique is simply due to the fact that, in a great number of the molecules studied to date, only one absorbing state lies within the wavelength range of available laser systems. Moore *et al.* have pumped the overtones of CO₂ and Casleton and Flynn have pumped both a fundamental and a hot band transition in COF₂.^{5,6} In this study, in addition to two different infrared active fundamentals being initially excited and the rates thus obtained compared, a third, "hot band" transition from either the ν_4 or ν_7 mode to a state(s) in the 2000 cm⁻¹ region has been excited. The studies involving each of these transitions have provided primary and supportive evidence in the deduction of mechanisms that populate the vibrational manifold of this molecule.

Recently, the rare gas dependence of *V-V* rates was proposed as a diagnostic technique to differentiate between resonant and nonresonant pathways and to extract specific rate constants from experimental data. The development of this technique was a direct outcome of studies on CH₂D₂.⁷ Succinctly stated, the rise rate of a state populated exclusively by a resonant transition that involves the collision of two vibrationally excited species shows little or no dependence of the rate upon added rare-gas pressure, whereas when nonresonant transitions are exclusively involved in filling a state, a linear increase in rise rate is observed upon addition of rare gas. For a pathway involving sequential resonant and nonresonant steps, the rate of filling of a state will increase upon addition of rare gas until the resonant step

^{a)}Alfred P. Sloan Fellow.

becomes rate limiting; at this point the rise rate will not be affected as the rare-gas pressure is further increased. This technique was successfully applied to the determination of the processes involved in populating the [ν_1 , ν_6], [ν_2 , ν_8], ν_3 , and ν_9 modes in CH₂D₂.

An additional method for the determination of $V-V$ energy transfer mechanisms, which was first applied to the CH₃F system, is also used in this study.⁸ In CH₂D₂/O₂ mixtures, following $V-V$ equilibration within the CH₂D₂ manifold, a decrease in fluorescence intensity from CH₂D₂ is observed due to intermolecular equilibration of O₂ with CH₂D₂. Under low excitation conditions and with rapid collisional equilibration of the vibrational manifold of the initially excited species, the decrease in fluorescence intensity is proportional to the amount of vibrational energy required for the final equilibration with O₂. This can be used to determine vibrational pathways in the initially excited species, in this case, CH₂D₂.

The basis for this technique lies in the fact that under the experimental condition described in Section II the energy needed to equilibrate the O₂ vibrational manifold with CH₂D₂ comes largely from the excited vibrational states of the absorbing species with the largest Boltzmann populations. Energy flows from these levels via a specific path into the vibrational manifold of O₂. All possible paths are characterized by the amount of vibrational and translational/rotational energy required to achieve the final equilibration. The decrease in fluorescence intensity of a CH₂D₂ state is proportional to the amount of vibrational energy transferred to O₂ and this can be quantitatively determined for any specific pathway. In CH₂D₂ this procedure was used to differentiate between resonant and nonresonant pathways as the means of filling the ν_3 mode.

The preceding techniques have furnished information through which the energy transfer pathways in CH₂D₂ have been deduced. The deduction of pathways has also allowed for the determination of a number of kinetic $V-V$ rate constants. Numerical modeling and theoretical calculations have been performed to confirm the proposed pathways and the results are fully consistent with experimental observations.

It is believed that these studies, both experimental and theoretical, provide a complete description of the energy transfer processes occurring among the vibrational states of CH₂D₂ below 3000 cm⁻¹.

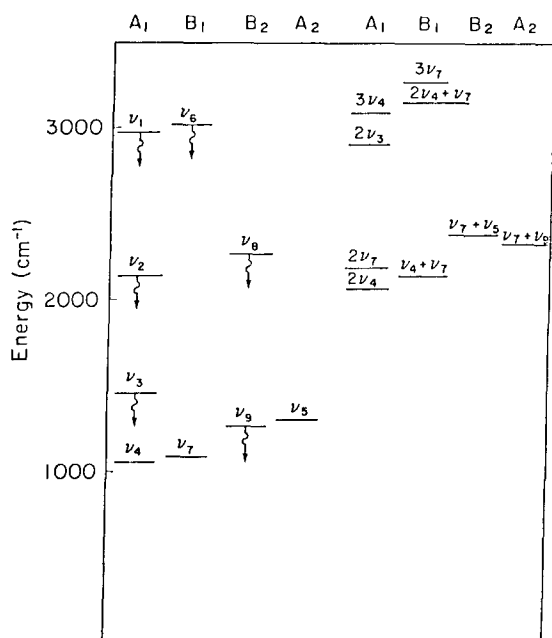
The remainder of this paper is organized in the following manner. In Sec. II the details of the experimental apparatus and conditions under which each experiment was performed are presented. Section III reports the results obtained using the methods mentioned previously. It should be noted that in this and subsequent sections the vibrational manifold of dideuteromethane has, for convenience, been divided into three regions. The lower region consists of the states between 1030 and 1450 cm⁻¹ (the ν_4 , ν_7 , ν_9 , ν_5 , and ν_3 fundamentals), the middle region consists of states between 2066 and 2600 cm⁻¹ (the ν_2 , ν_8 fundamentals as well as a number of overtones and combination bands), and the upper region contains states between 2900 and 3240 cm⁻¹ (the ν_1

and ν_6 fundamentals with overtones and combination bands). In Sec. IV the proposed energy transfer mechanisms are discussed with regard to the experimental findings and numerical studies are presented as supporting evidence for these mechanisms. A discussion of energy transfer calculations for the system is also included. Section V contains conclusions concerning the energy transfer pathways and dynamics in this molecule.

II. EXPERIMENTAL

The details of the experimental apparatus have been reported previously; however, a brief description will be provided here.^{3,9} In each experiment the time dependence of fluorescence from various states in CH₂D₂ was monitored subsequent to irradiation with either the $R(22)$, $P(24)$, or $P(38)$ lines of the 9.6 μ band of a CO₂ laser, Q -switched at 100 Hz. Identification of the lasing transitions was achieved by the use of a $\frac{1}{2}$ m grating monochromator that was calibrated against an Optical Engineering CO₂ Laser Spectrum Analyzer and a HeNe laser. The assignment of molecular transitions to each of these lines is based solely on spectroscopic considerations.² The $R(22)$ line at 1080 cm⁻¹ lies very near the dense ν_7 band center at 1090 cm⁻¹; therefore, this line is expected to cause a transition from the ground state to ν_7 . When CH₂D₂ is irradiated with the $P(24)$ laser line at 1043 cm⁻¹, an instantaneous rise in the population of states at 2000 cm⁻¹ followed by a fast fall (on a $V-V$ timescale) to near ambient is observed. The presence of only a very small amplitude $V-T/R$ equilibration step is an indication of the "hot band" nature of the induced transition. Neither upper nor lower levels of this hot band transition were directly determined. Spectroscopic and population considerations are suggestive of ν_4 or ν_7 as the most likely candidates for the lower state of this transition. The $P(38)$ laser line at 1029 cm⁻¹ excites population from the ground state and simultaneously causes a hot band transition. This is evidenced by the observation of an instantaneous rise in the population of states at 2000 cm⁻¹, followed by a double exponential fall corresponding to a partial equilibration of the manifold on the $V-V$ timescale followed by further $V-T$ equilibration. The overlap of $P(38)$ at 1029 cm⁻¹ with the dense ν_4 band center at 1033 cm⁻¹ suggests that the primary transition caused by this line is from the ground state of the molecule to ν_4 . As in the case of $P(24)$ excitation, the states involved in the hot band transition could not be uniquely identified but, again, it is very likely that the ν_4 or ν_7 level is the lower state of the transition.

The CO₂ laser pulse energy was typically 2 mJ, as measured by a calibrated thermopile, with a typical temporal width of 1.8 μ sec at the base [approximately 800 nsec full width at half-maximum FWHM]. Irradiation with a variety of other laser lines, including the $R(40)$, $R(8)$, $P(20)$, and $P(34)$ lines of the 9.6 μ branch, resulted in detectable, although weak, fluorescence. The fluorescence signals that resulted via irradiation with these lines were not subjected to further study. The strongest fluorescence signal was obtained using the $R(22)$ line.



Partial Energy Level Diagram of CH₂D₂

FIG. 1. Partial energy level diagram for states in CH₂D₂ below 3550 cm⁻¹.

The detector for a given experiment varied with the wavelength region under observation. With each detector, the output was amplified, digitized by a Biomation 610B transient recorder, and averaged by a hardwired signal averager. Rates and preexponentials were obtained from the averaged signals via Guggenheim or non-linear least-squares routines on either a Data General Nova 3 or CDC 6600 computer. A partial energy level diagram of CH₂D₂ is shown in Fig. 1. An In:Sb (Spectronics) detector was used for monitoring 3–5 μ fluorescence from the [ν_1, ν_6], ν_2 , and ν_8 states. The detector and its associated electronics had a response time of 0.83 μsec.⁹ Fluorescence from the ν_1 and ν_6 fundamentals could not be separated due to their proximity and the extensive rotational overlap of these states. A 3.01–4.00 μ bandpass filter was used to isolate fluorescence from these combined levels. Principally, the ν_2 state could be viewed using the In:Sb detector and either a 4.8 μ l. p. (long pass) or a 4.7 μ b. p. (bandpass) filter. These filter and detector combinations transmit in the 4.83–5.67 and 4.69–4.89 μ regions, respectively. Combined fluorescence from both the ν_2 and ν_8 states could be studied with a 4.5 μ l. p. filter with an effective spectral window of 4.39–5.67 μ (5% transmittance pts.).

The ν_3 mode at 6.90 μ was observed with a Au:Ge detector with a 5 kΩ resistive load looking through a 6.66–7.27 μ b. p. filter. The response time for this detector and associated electronics was 1.05 μsec.⁹

Fluorescence from the ν_9 mode was observed through a narrow bandpass filter that transmits in the 7.97–8.27 μ region using a liquid helium cooled, Cu:Ge detector and 5 kΩ resistive load. The detector and associated electronics were found to have a response time of 0.75 μsec.⁹ The ν_5 state is not infrared active and laser

scatter precluded observation of either the ν_4 or ν_7 fundamentals.

CH₂D₂ was obtained from Merck and Co. with a stated purity of 98%. It was shown by mass spectrometric analysis to have less than 1% impurities, mostly other deuterated methanes. Rare gases were purchased from Matheson Gas Products, as was the oxygen, with the following minimum purities: He, 99.9999%; Ne, 99.995%; Ar, 99.9995%; Kr, 99.9995%; Xe, 99.9995%; O₂, 99.99%. All gases were used without further purification. In experiments where a mixture of gases were used, a sufficient time was allowed for complete mixing.

All experiments were performed at ambient temperatures, 22 °C ± 1 °C.

III. RESULTS

For the sake of clarity we first provide a short qualitative description of the time dependence of the fluorescence signals observed from all states following excitation with each pump line. (See Fig. 2.)

R(22). All observed states: $\nu_9, \nu_3, [\nu_2, \nu_8], [\nu_1, \nu_6]$, exhibit a slow single exponential fall characteristic of the *V*-*T/R* equilibration of the molecule at a rate of 1 msec⁻¹ Torr⁻¹. ν_9 and [ν_2, ν_8] exhibit single exponential rises while [ν_1, ν_6] and ν_3 as shown in Fig. 2, exhibit clearly observable induction periods on their rises.

P(24). An immediate rise is observed from [ν_2, ν_8] followed by a fast (on a *V*-*V* timescale), single exponential fall. A fast single exponential rise and fall, both on a *V*-*V* timescale, is observed from [ν_1, ν_6]. Both ν_9 and ν_3 were too weak to detect. The characteristically slow *V*-*T/R* step had a small amplitude for this pump.

P(38). Fluorescence signal shapes from ν_9, ν_3 and [ν_1, ν_6] were nearly identical to the case of *R*(22) pump. [ν_2, ν_8] showed an instantaneous rise followed by a double exponential fall. The slow fall corresponded to the *V*-*T/R* deactivation of the molecule while the initial, fast fall was on a *V*-*V* timescale.

Table I presents the *V*-*V* and *V*-*T/R* rates for fundamentals in CH₂D₂ that were studied. *V*-*V* rates obtained via *R*(22) excitation have been reported previously but are included here for completeness. *V*-*T/R* deactivation rates with various rare-gas collision partners have been previously reported.³ All indicated *V*-*T/R* rates were determined using the *R*(22) pump over a pressure range of 0.1–25 Torr of CH₂D₂.

A. Lower region of the vibrational manifold ($\nu_4, \nu_7, \nu_9, \nu_5, \nu_3$)

Laser scatter precluded the direct observation of fluorescence from ν_4 and ν_7 due to their proximity to the exciting lines. ν_5 could not be directly studied since it is IR inactive.

Fluorescence from ν_9 was monitored following *R*(22) and *P*(38) irradiation. The signals were nearly identical in each case. The rise in fluorescence intensity from ν_9 was analyzed as a single exponential. From an inverse lifetime vs pressure plot a rate of 263 ± 12 msec⁻¹ Torr⁻¹

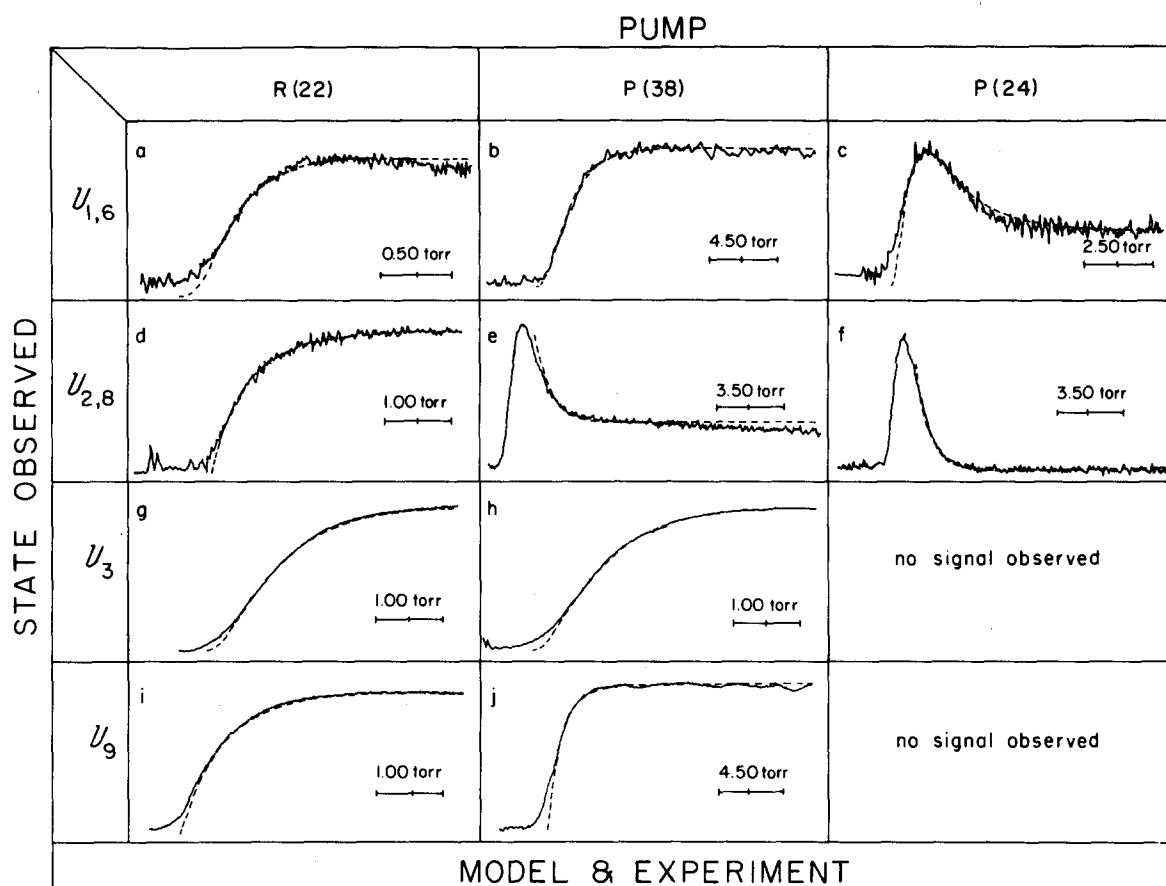


FIG. 2. Fluorescence signals from the observed states at pressures indicated for each of the three laser lines (solid line) with the temporal population evolution predicted by the full manifold model of Sec. IV E superimposed (dashed line). In Fig. 2(a) the total trace is of $128 \mu\text{sec}$ duration and the scale bar in the lower right corner spans $25 \mu\text{sec}$. In Figs. (b)–(j), the scale bar spans $5 \mu\text{sec}$. In (a)–(d) and (g)–(j), initial deviation of the model signal from the experimental signal is largely due to the response of the molecule to a laser pulse of finite width. The rises of signals (e) and (f) are faster than the response time limit. For signals (b) (e), (f), and (j), a correction was incorporated in the generated signals for the finite detection response time. This correction is negligible for the other signals pictured.

was obtained for the $R(22)$ pump and $250 \pm 40 \text{ msec}^{-1} \text{ Torr}^{-1}$ for the $P(38)$ pump. When the molecule was pumped with $P(24)$, the emission from this state was too weak to observe.

ν_3 was studied with $R(22)$ and $P(38)$ pumps. With either line, the fluorescence signals exhibited a distinct induction period, implying that the signal was the sum of a rapidly decreasing small amplitude exponential and a slowly increasing large amplitude exponential. Figure 3 shows a semilogarithmic plot of a typical signal (intensity vs time). It can be seen that at long times the contribution of the fast decreasing exponential to the total signal amplitude is negligible and the slope of the line in this region is a good approximation to the eigenrate of the slower, increasing exponential. By extrapolating this slow exponential to time zero (the time of the incident laser pulse) and subtracting the extrapolated values from the experimental signal, the points corresponding to the decreasing exponential can be obtained. From the slope of these points the eigenrate of this exponential is determined. For the increasing exponential the eigenrate was found to be $250 \pm 25 \text{ msec}^{-1} \text{ Torr}^{-1}$ and an eigenrate of $650 \pm 150 \text{ msec}^{-1} \text{ Torr}^{-1}$ was measured for the decreasing exponential. For ν_3 signals, when analyzed as single exponentials by analyzing points after

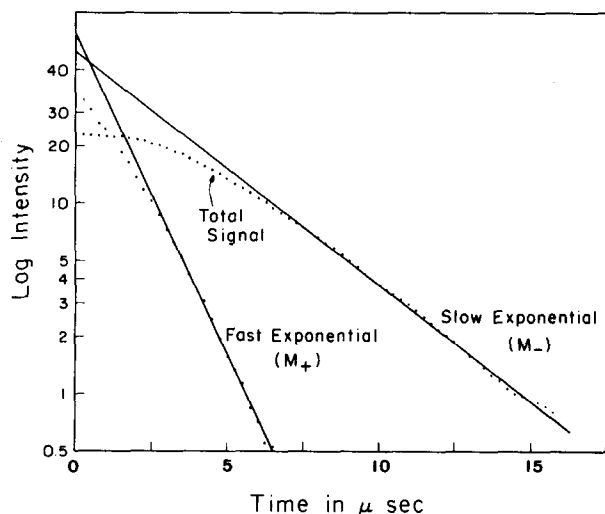


FIG. 3. Semilogarithmic plot of ν_3 fluorescence. The total signal points are the absolute values of the experimental data points after a base line subtraction. M_- is the slow exponential eigenrate, the eigenrate observed at long times when the contribution of the fast eigenrate to the total signal is negligible. M_+ , the fast eigenrate is determined from the absolute values of the differences between the slow exponential (M_-) extrapolated to short times and the corresponding total signal points. The CH_2D_2 pressure was 1.00 Torr .

TABLE I. V-V rates in CH₂D₂.

State(s)	Laser lines (9.6 μm branch)		
	P(38) ^a	R(22) ^b	P(24) ^c
ν ₉ rise	250 ± 40 ^d	263 ± 12	not observed
fall	V → T/R ^a	V → T/R ^e	
ν ₃ rise	190 ± 25	212 ± 21 ^f	not observed
fall	V → T/R ^e	V → T/R ^e	
[ν ₂ , ν ₈] rise	immediate	291 ± 29	immediate
fall	275 ± 35 ^g	V → T/R ^e	275 ± 35 ^g
[ν ₁ , ν ₆] rise	125 ± 15	130 ± 13 ^f	212 ± 25
fall	V → T/R ^e	V → T/R ^e	190 ± 30 ^g

^aP(38) initially excites the ν₄ mode and a hot band transition from a 1000 to 2000 cm⁻¹ state.

^bThe R(22) line excites the ν₇ mode.

^cP(24) excites a hot band transition from a 1000 cm⁻¹ state to a 2000 cm⁻¹ state.

^dAll rates are in msec⁻¹Torr⁻¹.

^eV → T/R rate was 1.00 ± 0.05 msec⁻¹Torr⁻¹.

^fReported values are with the points corresponding to an induction time neglected.

^gAlso contains a small amplitude slow V → T/R step. The rates for the rise and fall of these states were obtained via a biexponential nonlinear least-squares analysis of the experimental signals.

the induction period, a rate of 212 ± 21 msec⁻¹Torr⁻¹ was obtained for R(22) excitation and a rate of 190 ± 25 msec⁻¹Torr⁻¹ was obtained with a P(38) pump. These values are the same within experimental error. The rare-gas dependence of the rate of activation for the ν₃ and ν₉ modes were also obtained. Figure 4 illustrates the dependence of the rate upon Ne pressure for each of these levels. By varying the pressure of Ne from 0–30 Torr for a 1 Torr sample of CH₂D₂, the neon dependence of the rise rate of ν₃ was determined to be

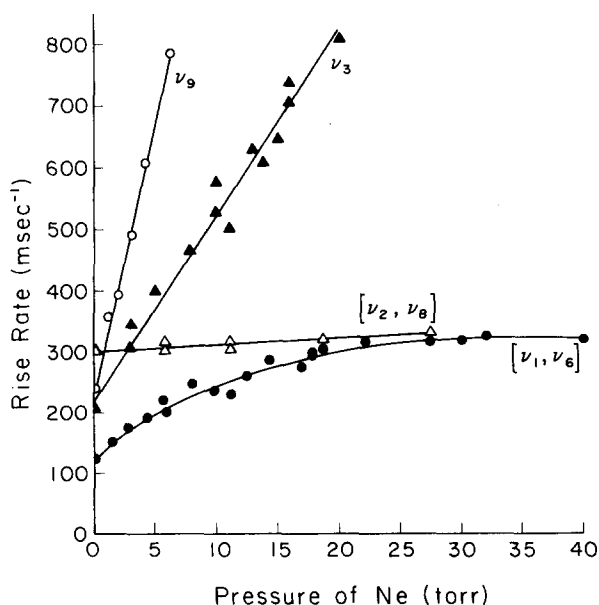


FIG. 4. Rare gas pressure dependence of the rise rates of [ν₁, ν₆] (●), [ν₂, ν₈] (Δ), ν₃ (▲), and ν₉ (○) for 1 Torr of CH₂D₂.

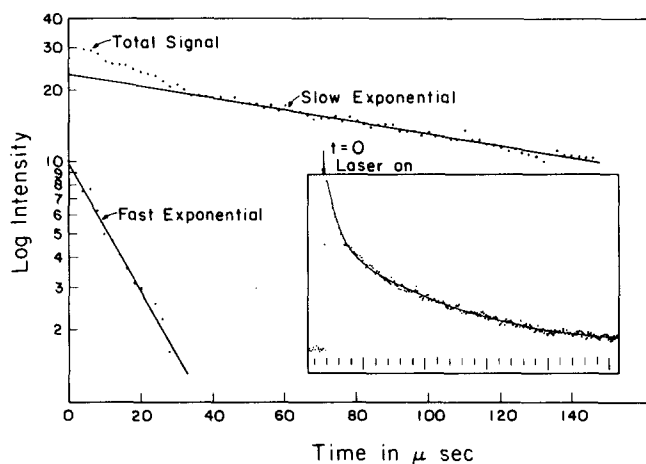


FIG. 5. Semilogarithmic plot of ν₃ fluorescence with the experimental fluorescence signal as an inset. The time base for the inset is 2 μsec/pt. or 512 μsec for the full signal. The plotted points are obtained in the same manner as in Fig. 3. The slow exponential is a result of V-T/R relaxation and the fast exponential is due to CH₂D₂-O₂ equilibration. The mixture contained 1.41 Torr CH₂D₂ and 29.90 Torr O₂. The fast exponential had a rate of 55.8 ± 5.3 msec⁻¹ which corresponds to a value of 13.6 ± 1.4 msec⁻¹Torr⁻¹ for the rate constant for the process indicated in Eq. (5c).

30 ± 3.5 msec⁻¹ (Torr Ne)⁻¹ while that of ν₉ was 80 ± 16 msec⁻¹ (Torr Ne)⁻¹. These rates are obtained by treating the observed signals as single exponentials.⁷

In order to ascertain the mechanism of filling ν₃, the time evolution of its population was monitored in CH₂D₂-O₂ mixtures following the R(22) pump. A double exponential fall was observed, characteristic of V-V equilibration between CH₂D₂ and O₂ followed by the V-T/R relaxation of the system. It has previously been demonstrated that the relative amplitudes of these exponentials can differentiate among various possible (V-V) mechanisms.⁸ This point will be further developed in Sec. IV. Figure 5 shows an experimental signal and its semilogarithmic plot. The observed rate for the fast process in Fig. 5 is 55.8 ± 5.3 msec⁻¹ for 1.41 Torr of CH₂D₂ and 29.90 Torr of O₂. Table II summarizes the experimental conditions and results of these studies.

B. Middle region of the vibrational manifold

The [ν₂, ν₈] state exhibits a nonresponse time-limited rise rate only with the R(22) pump. Its rate is 291 ± 29

TABLE II. Amplitude ratios (n^f/n⁰)-CH₂D₂/O₂ equilibration.

x _{O₂}	% decrease calculated ^a			Experimental
	Resonant	Nonresonant		
0.955	28	60		62
0.968	21	52		67
0.967	22	53		63
0.967	22	53		64
0.963	24	56		53
0.970	20	50		43

^aThe calculated nonresonant and resonant ratios were obtained with Eqs. (14) and (16) of the text, respectively.

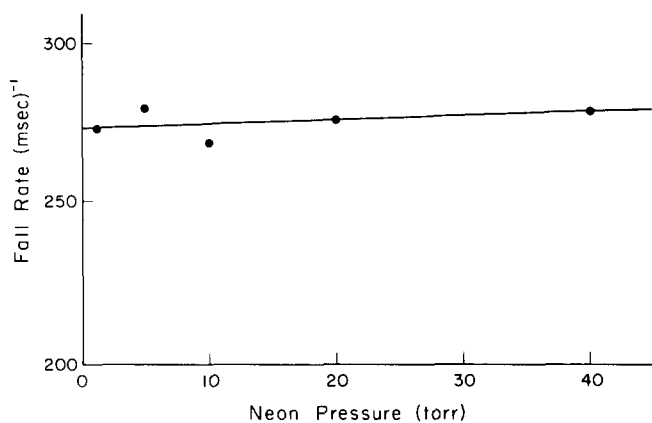


FIG. 6. Neon pressure dependence of the $[\nu_2, \nu_8]$ fall rate. The pressure of CH₂D₂ was 1.00 Torr. The exciting line was P(24).

msec⁻¹ Torr⁻¹. This rate proved to be nearly independent of the pressure of added rare gas (Ne) (see Fig. 4). Both P(24) and P(38) induce a direct transition to this region and therefore with these pumps $[\nu_2, \nu_8]$ exhibits an immediate rise in fluorescence intensity. Following pumping with P(24), these states relax, virtually completely, to their ambient population at a rate of 275 ± 35 msec⁻¹ Torr⁻¹. This relaxation rate was also found to be independent of Ne pressure (see Fig. 6). When pumped with the P(38) line, which is expected to simultaneously excite ν_4 and a state in the 2000 cm⁻¹ region, the fluorescence signal decays at the same rate as in the P(24) case to ~33% of its initial amplitude. This fast decay is followed by a slow V-T/R fall.

C. Upper region of the vibrational manifold

When analyzed as single exponentials, the rate of activation for the $[\nu_1, \nu_6]$ modes was measured at 130 ± 13 msec⁻¹ Torr⁻¹ with an R(22) pump and 125 ± 15 msec⁻¹ Torr⁻¹ with a P(38) pump. At low pressure, both sets of signals possessed an easily observable induction time. With a P(24) pump, the V-V rate of activation obtained was 212 ± 25 msec⁻¹ Torr⁻¹, with no apparent induction time, and the rate of V-V deactivation for the $[\nu_1, \nu_6]$ modes (i.e., its rate of equilibration with the rest of the manifold) was 190 ± 30 msec⁻¹ Torr⁻¹.

The plot of the rate of rise of $[\nu_1, \nu_6]$ vs Ne pressure displays an initial increase in rate upon increasing rare gas pressure, reaching a plateau of 330 ± 30 msec⁻¹ Torr⁻¹ at high rare-gas pressures (Fig. 4).

IV. DISCUSSION

A. $\nu_4, \nu_7, \nu_9, \nu_5,$ and ν_3 states

In the following, the kinetics of the $\nu_4, \nu_7, \nu_9, \nu_5,$ and ν_3 fundamentals will be discussed as a subsystem separate from the rest of the vibrational manifold and the perturbation that the remaining states have on these modes will be neglected. The validity of neglecting this perturbation rests on the fact that the remaining levels contain a relatively small portion of the total population of the excited state manifold.^{7,10} Separation

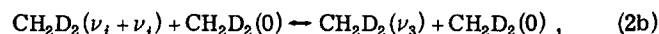
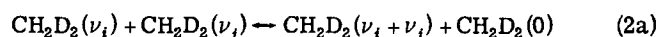
of ν_3 from the 2000 cm⁻¹ states and grouping ν_3 with the lower manifold may appear to be questionable; however, this treatment is justified *a posteriori*. In what follows, overwhelming evidence will be presented for the lack of significant direct V-V paths between ν_3 and the 2000 cm⁻¹ states. It will also be shown that ν_3 obtains virtually all of its population from states below it in the vibrational manifold and therefore the effect of rate processes within the upper or middle manifold on ν_3 are completely buffered by the large population of the lower states ($\nu_5, \nu_9, \nu_7, \nu_4$). This buffering effect has been verified by numerical modeling of the complete manifold.

Since ν_3 fills faster than states in the 3000 cm⁻¹ region, even in the absence of rare gas, it is easy to rule out pathways such as those shown in Eq. (1) for the filling of ν_3 .

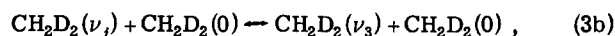


where $i=1, 6$. In a mechanism where a state is populated through a high-lying state with an equilibrium population much smaller than the final state (known as an "around-the-horn" mechanism), the filling of the final state is inefficient and, in this case [Eq. (1)], would at best predict ν_3 to rise at a rate two orders of magnitude slower than that of the rise of $[\nu_1, \nu_6]$.⁷

Two other possible mechanisms for populating the ν_3 fundamental in CH₂D₂ are more plausible. The first involves a resonant step to a state or states in the 2000 cm⁻¹ region, followed by an exoergic crossover to ν_3 :



where i or $j=4, 7, 9,$ or 5 and the second is a non-resonant transfer of energy from the fundamentals below the ν_3 state:



where $i=4$ or 7 and $j=9$ or 5 .

As suggested by the inclusion of the ν_3 mode in the lower manifold, it is our belief that the nonresonant process [Eq. (3)] is responsible for the filling of the ν_3 mode. This hypothesis is supported by a variety of observations.

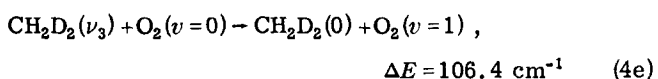
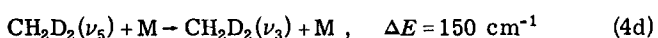
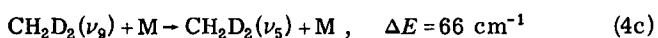
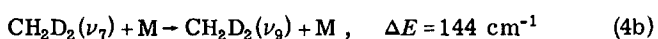
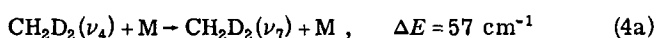
The V-V rate of activation of the ν_3 mode varies linearly with added rare gas as shown in Fig. 4. This behavior is only consistent with that of a state being exclusively filled by nonresonant processes. Moreover, since Ne linearly accelerates the rate of rise of ν_3 to values much above the filling rate of $[\nu_2, \nu_8]$ (which is independent of Ne pressure, (see Fig. 4), Eq. (2) can be confidently refuted in favor of Eq. (3).

A second and independent proof for the nonresonant path as the means of populating the ν_3 mode was obtained through the study of the intermolecular equilibration of CH₂D₂ with O₂. As done previously for CH₃F/O₂ mixtures, the percentage decrease in fluorescence intensity of a mode in CH₂D₂ as the molecule equilibrated with oxygen was used to limit the number of possible

pathways for the activation of ν_3 .⁸

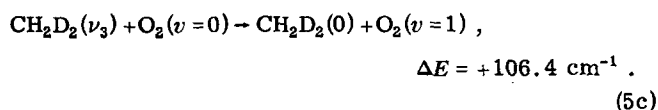
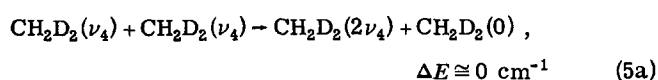
The $v=1$ level of O₂ lies at 1556.4 cm⁻¹ and the ν_3 level of CH₂D₂ at 1450 cm⁻¹. Due to their proximity, it is expected that the $v=1$ level of O₂ comes into $V-V$ equilibrium with CH₂D₂ via energy transfer from the ν_3 level of CH₂D₂. This transfer is slow compared to the rapid $V-V$ equilibration of the CH₂D₂ manifold, requiring collisions of the type of Eq. (4e). In turn, the energy that is transferred to O₂ from the ν_3 level arrives there almost exclusively from the lower levels of the CH₂D₂ manifold either by resonant or nonresonant processes. This can easily be verified by a consideration of the relative Boltzmann populations of the CH₂D₂ levels. It is important to note that the low excitation source used in these studies does not significantly perturb these lower levels in CH₂D₂ from their ambient Boltzmann populations.

Specific resonant and nonresonant paths were postulated and the percentage decrease in fluorescence intensity of the ν_3 mode that would be expected as CH₂D₂ equilibrates with O₂ was calculated. The nonresonant pathway considered was one in which energy was drawn from the equilibrated states, the ν_4 , ν_7 , ν_9 , ν_5 , and ν_3 levels of CH₂D₂ and transferred through the ν_3 state to O₂:



where M is either CH₂D₂ or O₂ or a rare gas. Since energy transfer to O₂ is slow compared to the equilibration of the CH₂D₂ manifold, all the states in the lower manifold of CH₂D₂ are expected to be coupled among themselves on the timescale of this transfer. This is virtually assured by the addition of rare gas to the CH₂D₂/O₂ mixture. The added rare gas speeds up most CH₂D₂ internal nonresonant $V-V$ steps relative to CH₂D₂-O₂ $V-V$ transfer. However, in this case the presence of added rare gas did not affect the experimentally determined rates or amplitudes implying that the CH₂D₂ states that contained significant population were already equilibrated on the timescale of $V-V$ transfer to O₂. As will be seen later, in the low excitation regime, for any nonresonant path involving all the states specified in Eq. (4), the population of all states will decrease by the same fractional amount.

The choice of a resonant pathway is not as obvious. One choice is the following:



The total vibrational and translational energy changes for the nonresonant [Eq. (4)] and resonant paths [Eq. (5)] are

$$E_{\text{vib}} = -1033 \text{ cm}^{-1}, \quad E_{\text{trans}} = -523.4 \text{ cm}^{-1},$$

and

$$E_{\text{vib}} = -2066 \text{ cm}^{-1}, \quad E_{\text{trans}} = +500.6 \text{ cm}^{-1},$$

respectively. The important difference in the preceding two paths is that the resonant path requires two quanta of initial excitation to populate the O₂ ($v=1$) mode whereas the nonresonant path requires only one. This is reflected in the percentage decrease in the intensity of ν_3 fluorescence upon equilibration with O₂.

The following procedure is used to quantitatively determine the percentage decrease in intensity of population of ν_3 . Considering n to be the number of molecules initially excited by the laser, population balance equations can be written for the nonresonant and resonant paths, respectively:

$$\begin{aligned} n &= n_{\nu_4}^0 + n_{\nu_7}^0 + n_{\nu_9}^0 + n_{\nu_5}^0 + n_{\nu_3}^0 + n_{\text{O}_2}^0(v=1) \\ &= n_{\nu_4}^f + n_{\nu_7}^f + n_{\nu_9}^f + n_{\nu_5}^f + n_{\nu_3}^f + n_{\text{O}_2}^f(v=1) \end{aligned} \quad (6)$$

and

$$\begin{aligned} n &= n_{\nu_4}^0 + 2[n_{2\nu_4}^0 + n_{\nu_3}^0 + n_{\text{O}_2}^0(v=1)] \\ &= n_{\nu_4}^f + 2[n_{2\nu_4}^f + n_{\nu_3}^f + n_{\text{O}_2}^f(v=1)], \end{aligned} \quad (7)$$

where $n_{\nu_i}^0$ is the deviation from ambient population for mode ν_i after internal $V-V$ equilibration in CH₂D₂ but before equilibration with O₂ and $n_{\nu_i}^f$ is the population of state ν_i after equilibration with O₂. Of course, $n_{\text{O}_2}^0(v=1)$ is zero. For the nonresonant path it is possible to show that the population deviations are related in the following manner,

$$n_{\nu_i} = n_{\nu_j} (g_i/g_j) \exp[(E_j - E_i)/kT], \quad (8)$$

where g_i indicates the degeneracy of state ν_i , while E_i is the energy. The population deviation of the oxygen $v=1$ state can be expressed by

$$N_{\text{O}_2}(v=1) = n_{\nu_i} \left(\frac{N_{\text{O}_2}^0(v=0)}{N_{\text{O}}^0} \right) g_i \exp \left(\frac{E_i - E_{\text{O}_2}(v=1)}{kT} \right), \quad (9)$$

where $N_{\text{O}_2}^0(v=0)$ is the ambient population of the ground state of oxygen and N_{O}^0 is that of the CH₂D₂ ground state. The ratio of ground state populations may be closely approximated by the ratio of the mole fractions present in the mixture

$$X_{\text{O}_2}/(1 - X_{\text{O}_2}), \quad (10)$$

where X is the mole fraction of O₂. There is an important difference between the equation relating the population deviations of the states that come into equilibrium via excited state-excited state collisions and those described by Eq. (8). The relationship for the population deviations of states equilibrated via excited state-excited state collisions of the type illustrated in Eq. (5a) is

$$n_{2\nu_i} = 2n_{\nu_i} \exp[(E_i - E_{2i})/kT]. \quad (11)$$

The factor of 2 arise from the stoichiometry of processes of the type represented by Eq. (5a).

Substituting Eqs. (9)–(11) into the population balance equations and rearranging provides the following equations for the nonresonant and resonant pathways, respectively:

$$\frac{n_{\nu_3}^f}{n_{\nu_3}^0} = \frac{1 + \exp[(E_{\nu_3} - E_{\nu_4})/kT] + \exp[(E_{\nu_3} - E_{\nu_7})/kT] + \exp[(E_{\nu_3} - E_{\nu_9})/kT] + \exp[(E_{\nu_3} - E_{\nu_5})/kT]}{1 + \exp[(E_{\nu_3} - E_{\nu_4})/kT] + \exp[(E_{\nu_3} - E_{\nu_7})/kT] + \exp[(E_{\nu_3} - E_{\nu_9})/kT] + \exp[(E_{\nu_3} - E_{\nu_5})/kT] + [X_{O_2}/(1 - X_{O_2})] \cdot \exp\left(\frac{E_{\nu_3} - E_{O_2}(v=1)}{kT}\right)} \quad (12)$$

$$\frac{n_{\nu_3}^f}{n_{\nu_3}^0} = \frac{\exp[(E_{\nu_3} - E_{\nu_4})/kT] + (4) \exp[(E_{\nu_3} - E_{2\nu_4})/kT] + (4)(1)}{\exp[(E_{\nu_3} - E_{\nu_4})/kT] + (4) \exp[(E_{\nu_3} - E_{2\nu_4})/kT] + (4)(1) + (4)[X/(1 - X_{O_2})] \exp[(E_{\nu_3} - E_{O_2}(v=1))/kT]} \quad (13)$$

These fractions are the ratio of the population deviation in the ν_3 mode after equilibration to that before equilibration with O₂ and are equal to the experimentally measured quantity, the ratio of the fluorescence intensity after equilibration to that before equilibration with O₂. Since in the low excitation regime the population deviations for the different states are linearly related [cf. Eqs. (8) and (9)], the ratio n^f/n^0 will be the same for all states involved in the energy transfer process. At 295 °K, Eqs. (12) and (13) reduce to the following for nonresonant and resonant pathways, respectively:

$$\frac{n_{\nu_3}^f}{n_{\nu_3}^0} = \left(1 + \frac{X_{O_2}}{(1 - X_{O_2})} 0.0308\right)^{-1} \quad (14)$$

$$\frac{n_{\nu_3}^f}{n_{\nu_3}^0} = \left(1 + \frac{X_{O_2}}{(1 - X_{O_2})} 0.201\right)^{-1} \quad (15)$$

Although the choice of the states involved in the nonresonant process was an obvious one, that is not the case with the resonant pathway. It was postulated that the states in the 2000 cm⁻¹ region are equilibrated and therefore are all involved in the transfer process. However, their contribution to the vibrational heat capacity of the system is small and the addition or neglect of these states in the calculation will not significantly affect the ratios in Eqs. (14) and (15). It is also quite possible that, instead of the process outlined in Eq. (5), all the states in the lower manifold are involved in the transfer of energy through ν_3 into O₂ in the resonant mechanism. If all states below 2900 cm⁻¹ are assumed to be involved in the energy transfer with oxygen, through ν_3 , the equation for the fractional decrease in fluorescence intensity is found to be

$$\frac{n_{\nu_3}^f}{n_{\nu_3}^0} = \left(1 + \frac{X_{O_2}}{(1 - X_{O_2})} 0.124\right)^{-1} \quad (16)$$

Of all resonant pathways, this resonant pathway would provide a fractional decrease closest to the nonresonant pathway.

The experimental signal is shown in Fig. 5. The slow, $V-T/R$, exponential fall is extrapolated to t_0 , the time of the laser pulse, as is the fast, $V-V$, exponential fall. The ratio of the amplitude of the slow exponential fall to the amplitude of the fast exponential fall at t_0 is the experimentally determined value for $n_{\nu_3}^f/n_{\nu_3}^0$.

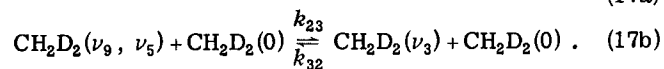
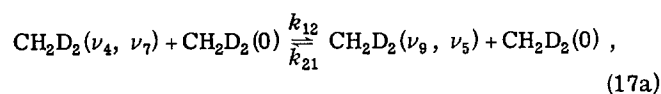
The percentage decrease in intensity of fluorescence originating from the ν_3 fundamental upon intermolecular equilibration with oxygen is presented in Table II for various mole fractions of oxygen. The calculated values for the nonresonant and resonant paths were obtained

using Eqs. (14) and (16), respectively. The percentage decreases obtained experimentally are easily seen to be inconsistent with the resonant path postulated for populating the ν_3 fundamental. Therefore, as explained in the preceding discussion, they are also inconsistent with any possible resonant path that might be responsible for filling the ν_3 mode. The deviations of the experimental values from the calculated nonresonant values are within the range of error associated with the determination of the initial amplitude of the two exponentials. Therefore, they are consistent with the rare-gas-dependent studies of the filling of ν_3 and the path of filling ν_3 involves nonresonant transition from the 1000 cm⁻¹ region as illustrated in Eqs. (4a)–(4d) or (3a) and (3b).

Further support for the nonresonant path filling ν_3 comes from studies involving the hot band pumps. These involve transitions from one of the states in the lower manifold to one of the states in the 2000 cm⁻¹ region. The immediate rise in population of [ν_2 , ν_8] induced by either the $P(24)$ or $P(38)$ laser lines decays at a rate of 275 ± 30 msec⁻¹ Torr⁻¹ which, within experimental error, is the observed rise rate of [ν_2 , ν_8] when ν_7 is initially excited with the $R(22)$ pump. With $P(24)$ excitation, no fluorescence is observed from ν_3 in contrast to the cases where either ν_4 or ν_7 are initially excited. These observations imply that [ν_2 , ν_8] is strongly coupled to ν_4 and ν_7 . If there is any direct flow of energy from [ν_2 , ν_8] to ν_3 it is much less efficient than the coupling of ν_3 to the lower manifold such that no significant excess population develops in ν_3 when only [ν_2 , ν_8] is directly pumped. Since the major population pathway for the ν_3 fundamental is a nonresonant process and the 2000 cm⁻¹ states are not filled directly from ν_3 , it is possible to view the states we have termed the lower manifold as a kinetically separate system from the rest of the vibrational manifold behaving essentially as indicated in Eq. (4). The possibility that the ν_3 mode is populated directly from the ν_7 or ν_4 states and not through the sequential process indicated in Eq. (4) will be discussed in Sec. IV E.

There are some simplifications of the sequential process for filling ν_3 that are suggested by experimental observations. The first of these involve the coupling between the ν_4 and ν_7 fundamentals. Due to their proximity and extensive rotational overlap they would be expected to equilibrate rapidly on the timescale of the experiment. That the measured activation rate for a state is the same within experimental error using either the

ν_4 or ν_7 modes as the initially excited state suggests that this assumption is correct. Therefore, the kinetic behavior of this system may be adequately explained by considering the ν_4 and ν_7 levels to be a single state with double degeneracy. Similar considerations for the ν_9 and ν_5 states lead us to believe that these states may also be adequately treated as one doubly degenerate state. The Schwartz, Slawsky, and Herzfeld (SSH) calculations done on this system also suggest that this approximation is a valid one since the magnitude of the SSH calculated rates for these steps are larger than the rates connecting the states not considered coupled in our model. In addition, for the states considered as single doubly degenerate states, there is overlap of rotational manifolds, which would tend to enhance the rate of coupling between these states over what is calculated via SSH theory. These assumptions and the range of their validity will be further discussed in Sec. IV E. These simplifications allow the lower manifold in CH₂D₂ to be adequately approximated as a three level system.



A detailed consideration of the effect of the finite rate of coupling of ν_4 , ν_7 and ν_9 , ν_5 as well as the possibility of parallel equilibration pathways for the $[\nu_4, \nu_7] \rightarrow [\nu_9, \nu_5]$ and $[\nu_9, \nu_5] \rightarrow \nu_3$ transitions will be considered in more detail in Sec. IV E in light of the restrictions imposed on the behavior of the system as a consequence of its experimentally observed behavior.

A three level system can be solved analytically.¹¹ The temporal evolution of the population in a level is a sum of two exponentials. For ν_3 , this corresponds to a slowly increasing and a rapidly decreasing exponential. The eigenrate (M_-) associated with the increasing exponential and the eigenrate (M_+) of the fast, decreasing exponential are given by the following formulas:

$$M_{\pm} = \frac{1}{2} \{S \pm (S^2 - 4A)^{1/2}\}, \quad (18)$$

where

$$S = k_{12} + k_{21} + k_{23} + k_{32},$$

$$A = k_{12} k_{32} + k_{12} k_{23} + k_{21} k_{32}.$$

The experimentally obtained values for M_+ and M_- are 650 ± 150 and 250 ± 25 msec⁻¹ Torr⁻¹, respectively (see Fig. 3). Using these values the individual rate constants k_{ij} may be determined from Eq. (18). There are only two independent rate constants in the equation as k_{ij} is related to k_{ji} through detailed balancing. In this system, SSH calculations, as to be discussed later, appear to be a good indication of relative $V-V$ rates. This suggests that $k_{32} > k_{21}$. Then the calculated rate constants may be assigned as follows: $340 < k_{32} < 520$ and $200 < k_{21} < 250$.

The wide spread of possible rates for k_{32} is due to the large error associated with the experimental value M_+ , the fast fall eigenrate.

The preceding three level model for the lower mani-

TABLE III. SSH rates for off-resonant intermode $V-V$.^a

	ν_4^b	ν_7	ν_9	ν_5	ν_3	ν_2	ν_8	ν_1	ν_6
ν_4		323	66	18					
ν_7			172	50	10				
ν_9				422	100				
ν_5					333				
ν_3									
ν_2							78		
ν_8									
ν_1									182
ν_6									

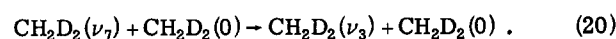
^aAll rates reported in msec⁻¹ Torr⁻¹.

^bWhere 323 is the forward rate constant of process $\text{CH}_2\text{D}_2(0) + \text{CH}_2\text{D}_2(\nu_4) + \text{CH}_2\text{D}_2(\nu_4) \rightarrow \text{CH}_2\text{D}_2(0) + \text{CH}_2\text{D}_2(\nu_2)$.

fold does not consider direct processes of the type



and



Although these processes should occur, they probably do so to a negligible extent due to the large energy gap between the $[\nu_4, \nu_7]$ and ν_3 states. This is reflected in the small rate constants calculated by SSH theory (Table III). These calculations will be discussed more fully in Sec. IV D. As further proof that direct energy transfer from the ν_4 or ν_7 state into the ν_3 mode is negligible, it is important to note that in the rise of the ν_3 fluorescence there is an initial period where the signal rises much more slowly than at later times. This "induction period" is predicted by the solution of the three level system for this state.¹¹ If any significant contribution to the population of the ν_3 mode was made through direct transfer from the ν_4 or ν_7 state ($k_{\nu_3-\nu_4,7} > 10$ msec⁻¹ Torr⁻¹), it can be shown through numerical modeling that this induction period would not be observable. Therefore, the filling of the ν_3 mode and the behavior of the lower manifold is consistent with the processes in Eq. (17). The identity and the magnitudes of possible parallel pathways involved in equilibration processes in the lower manifold will be further discussed in Sec. IV E. The signals generated via a three level system model of the lower manifold and the experimentally observed signals are in excellent agreement, as discussed in Sec. IV E and illustrated in Fig. 2.

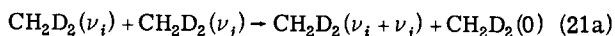
B. 2000 cm⁻¹ states

The 2000 cm⁻¹ states are the ν_2 and ν_8 fundamentals and a number of overtones and combination bands of the fundamentals in the lower manifold. These states are sufficiently close in energy to provide a high density of states in this region. Accordingly, it is expected that most, if not all, of these states are rapidly coupled. This assumption is supported by a comparison of the signals and rise rates obtained when viewing fluorescence from the 4.39–5.67, 4.69–4.89, and 4.83–6.57 μm wavelength regions subsequent to excitation of the ν_7 fundamental. For each wavelength interval, the

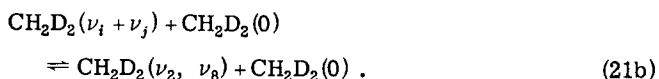
qualitative shape of the fluorescence signal and the measured activation rates were the same. If the ν_2 and ν_8 fundamentals possessed dissimilar rise rates and the rate coupling the two states was slow, the shape and activation rate of the fluorescence signal would be expected to change significantly as the viewed region changed from 4.83–6.57 μm , where the fluorescence originates almost totally from the ν_2 fundamental, to the 4.39–5.67 μm interval where fluorescence from both the ν_2 and ν_8 states is transmitted. Though convincing, this argument is not conclusive because ν_8 is the strongest emitter in the 2000 cm^{-1} region with an absorption coefficient over twice that of ν_2 . Additionally, the wings of ν_8 rotational manifold overlap those of the ν_2 manifold, thus some ν_8 emission may be detected with all of the above-mentioned filter combinations.²

More direct proof of the rapid coupling of the states in this region is provided by the studies utilizing the two CO₂ laser lines that induce a hot band transition, the P(38) and P(24) lines of the 9.6 μm branch. Fluorescence was viewed in the 4.39–5.67 μm wavelength region, originating from both the ν_2 and ν_8 states. For CH₂D₂ pressures down to 1.00 Torr, with either laser line pump, an immediate rise followed by a single exponential fall was observed: the later characteristic of V–V equilibration of these states with the lower manifold. Two possibilities may be considered: the hot band induces a transition directly to the observed state or it induces a transition to a neighboring overtone or combination band. In either case the initially excited state would undergo a rapid equilibration with the neighboring states prior to equilibration with the lower manifold. The absence of a second exponential fall for the first case and a rise for the second, can only be explained in light of other observations by the extreme rapidity of coupling of states in this region. It can be safely assumed that this equilibration rate at 1 Torr is greater than 1200 msec^{-1} , the response time of the detection system.

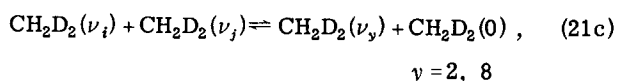
The direct evidence of a rapid nonresonant transfer between an overtone or combination band to the $[\nu_2, \nu_8]$ state suggests that when the ν_7 fundamental is initially excited and no hot band transition occurs, the $[\nu_2, \nu_8]$ state may become populated through a process involving a resonant step from a state at approximately 1000 cm^{-1} to an overtone or combination band in the 2000 cm^{-1} region; i. e.,



where i or $j=4, 7, 9, 5$, followed by the nonresonant step discussed previously,



The resonant process in Eq. (21a) is expected to be preferred over a direct resonant transfer to ν_2, ν_8 [as in Eq. (21c)] due to the larger quantum number change required in the process of Eq. (21c).



In either case the kinetics of the overall process do not

change as long as the process in Eq. (21b) is rapid. The above-mentioned mechanism is also verified through the study of the rare-gas dependence of the rise rate of the $[\nu_2, \nu_8]$ state. To review the logic underlying this procedure, the rate of a nonresonant transition is accelerated upon addition of rare gas; the rate of a resonant transition is not. When a mechanism is composed of both resonant and nonresonant processes, the observed rate will be accelerated until the resonant rate is rate limiting if it is not already rate limiting. If it is already rate limiting the observed rate will be independent of rare gas pressure.⁷ Figure 4 illustrates that, within experimental error, the rate of rise of the $[\nu_2, \nu_8]$ state is independent of rare-gas pressure.

A resonant transition is involved in populating the $[\nu_2, \nu_8]$ state, as shown by the rare-gas independence of the rise of the $[\nu_2, \nu_8]$. Since the final state in this resonant transition is most likely to be an overtone or combination band in the 2000 cm^{-1} region, there would then be a nonresonant transition from this overtone or combination band to the $[\nu_2, \nu_8]$ state. The rate of the nonresonant transition is faster than the rate of the resonant step, as evidenced by the independence of the rise rate of the $[\nu_2, \nu_8]$ state with respect to rare-gas pressure and by the rapid rate of activation of the $[\nu_2, \nu_8]$ state that was observed in the hot band transition studies. From this and our other observations, it is believed that the mechanism illustrated in Eqs. (21a) and (21b) is most assuredly the mechanism responsible for populating the $[\nu_2, \nu_8]$ mode. There does remain some ambiguity, however, as to which states, the ν_4, ν_7, ν_9 , or ν_5 , participate in the resonant transition [Eq. (21a)]. There is no reason, *a priori*, to believe that all the states in the 1000 cm^{-1} region are not simultaneously involved in resonant transitions providing multiple, parallel channels for populating the 2000 cm^{-1} states from the 1000 cm^{-1} states. However, transfer from $[\nu_9, \nu_5]$ to the 2000 cm^{-1} states does not represent a major pathway, since, if it did, then a pronounced rare gas dependence of the rise of $[\nu_2, \nu_8]$ would be expected. Interestingly, though, as shown in Sec. IV E, some coupling between $[\nu_9, \nu_5]$ and $[\nu_2, \nu_8]$ is required to prevent a decrease in the rise rate of $[\nu_2, \nu_8]$ as rare gas is added to the system and the rate of equilibration between $[\nu_4, \nu_7]$ and $[\nu_9, \nu_5]$ increases.

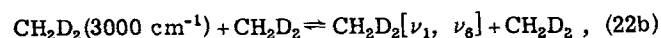
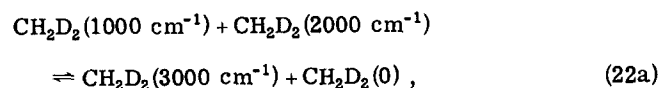
When viewing fluorescence from the $[\nu_2, \nu_8]$ state with the P(38) or P(24) pumps the signals illustrated in Fig. 2 are obtained. The measured fall rates of these signals are, within experimental error, the same as the rise of fluorescence observed from $[\nu_2, \nu_8]$ when ν_7 is pumped. That this situation corresponds to a reversal of the processes of Eq. (21) is further verified by the fact that these fall rates are independent of added rare-gas pressure. Figure 6 illustrates this for the P(24) pump. That the V–V fall from $[\nu_2, \nu_8]$ decays to different amplitudes with P(24) and P(38) pumps is an observation that can be quite easily rationalized upon consideration of the proposed mechanism and the various transitions that these lines excite. With the P(24) line, a small percentage of the population in the 1000 cm^{-1} states is excited to the 2000 cm^{-1} states. This creates a population deficit in the 1000 cm^{-1} states (less population than

the ambient population) and this deficit is remedied as population is transferred back into the 1000 cm⁻¹ states, a process that is responsible for the rapid V-V fall in the [ν_2 , ν_8] signals. Since the population deficit in the 1000 cm⁻¹ state is approximately equal to the population excited to the 2000 cm⁻¹ states, the [ν_2 , ν_3] signal decays to close to the initial intensity as most of the population that was excited is transferred into the 1000 cm⁻¹ states. On the other hand, in addition to a hot band transition, the P(30) line excites a transition from the ground state to one of the 1000 cm⁻¹ states, the ν_4 fundamental. This additional transition helps remedy the deficit in the 1000 cm⁻¹ states created by the hot band transition. It also raises the vibrational temperature of the system more than in the case of the P(24) pump and, therefore, less population than was excited into the 2000 cm⁻¹ region is required to be transferred into the 1000 cm⁻¹ states in order to restore the populations to a level mandated by the vibrational temperature of the system. As a result, the population in the 2000 cm⁻¹ states will remain above the ambient level and the V-V fall will not decay to as near the original intensity as with the P(24) pump. The consistent interpretation of all of the above observations gives a high degree of credibility to the proposed mechanism of Eqs. (21a) and (21b).

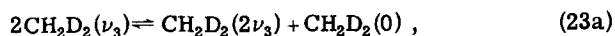
C. [ν_1 , ν_6] state

Fluorescence from the ν_1 and ν_6 states could not be separated due to the proximity of these states. Thus they will be treated as one doubly degenerate state. Since the [ν_1 , ν_6] state, at approximately 3000 cm⁻¹, is far removed in energy from the initially excited states, it is intuitively expected that resonant transitions are involved in its population pathway. The rare-gas dependence of the rise of this state is extremely interesting in that it shows that not only are resonant transitions involved but nonresonant transitions also participate in populating the [ν_1 , ν_6] state. Figure 4 presents the rare-gas dependence of the rise of the [ν_1 , ν_6] state. At lower pressures of rare gas the rate of activation of the [ν_1 , ν_6] state increases linearly with increasing rare-gas pressure. As previously explained, this initial increase is due to the acceleration of a nonresonant step in a mechanism consisting of both resonant and nonresonant steps. At higher pressures of rare gas the resonant step limits the rate of filling of the [ν_1 , ν_6] state and the leveling behavior of the rise vs rare-gas pressure is seen.

Two pathways are consistent with the observed rare-gas dependence of the [ν_1 , ν_6] rise. The first involves a state or states in the 2000 cm⁻¹ region,



and the second is a pathway involving the ν_3 fundamental,



Both mechanisms contain resonant and nonresonant transitions and would be expected to exhibit the type of rare-gas dependence of the rise rate seen experimentally. The implications of the rare-gas dependent experiments have previously been reported in great detail in Ref. 7. The conclusions derived therein are concisely reiterated here for completeness. The rate limit and initial slope of the rise in [ν_1 , ν_6] are compatible over the entire range of rare-gas pressure only with the mechanism of Eq. (23). Therefore in the presence of rare gases the dominant channel for populating [ν_1 , ν_6] is that of Eq. (23). However, considering only the rare gas dependent behavior, either mechanism, Eqs. (22) and (23), can account for the filling of [ν_1 , ν_6] in neat CH₂D₂. The extent of participation of each of these mechanisms in neat CH₂D₂ is further quantified below and in the numerical model section by comparison of the signals from this state obtained with the three different pumps with results of the numerical model.

The [ν_1 , ν_6] signal obtained with the R(22) pump initially exciting the ν_7 fundamental possessed a rise, the rate of which was determined to be 130 msec⁻¹ Torr⁻¹. The identical signal shape and rate, within experimental error, was obtained with the P(38) line, which initially excites the ν_4 fundamental as well as a hot band transition. A quite different signal was obtained using the P(24) line, which only induces a hot band transition. This signal consisted of a rise with a rate greater than that measured for this state using the R(22) or P(38) line. The rise was followed by a rapid V-V fall. Since with the P(24) pump, the 2000 cm⁻¹ states are instantaneously excited, the rapid rise is easily explained as the result of transfer originating from a state or states in the 2000 cm⁻¹ region [Eq. (22a)]. In this case the ν_3 pathway [Eq. (23)] cannot be important in populating [ν_1 , ν_6] since with a P(24) pump no significant excess population is developed in ν_3 . The V-V fall observed with the hot band pump is the result of the [ν_1 , ν_6] state equilibrating with the lower manifold since [ν_1 , ν_6] is populated before vibrational equilibration is achieved in the lower manifold. It is notable that the rate of this V-V fall is approximately equal to the rise rate of the ν_3 fundamental when the molecule is initially excited from below, 212 msec⁻¹ Torr⁻¹. However, the fall rate is due to a convolution of the processes that drain population out of [ν_1 , ν_6], a major process being the equilibration of [ν_1 , ν_6] with ν_3 via Eq. (23b) followed by process (23a) and subsequent equilibration of ν_3 with the rest of the lower manifold. Numerical modeling indicates that even in the absence of the aforementioned [ν_1 , ν_6] - ν_3 equilibration process, [ν_1 , ν_6] would still fall since it is coupled to the 2000 cm⁻¹ states that equilibrate with the lower manifold via the pathway of Eq. (22a). Numerical modeling also indicates that under the actual kinetic conditions that we believe govern population evolution in CH₂D₂, the latter pathway is present but is not as important as the former pathway in governing the fall of [ν_1 , ν_6].

It is now possible to interpret the experiments performed with P(38) excitation. In this case ν_4 and a 2000 cm⁻¹ state are simultaneously excited and therefore the channels of both Eqs. (22) and (23) are available for

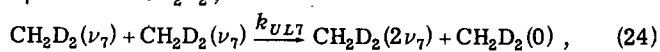
populating [ν_1 , ν_6]. This experiment serves as an absolute comparison of the efficiencies of these two pathways. The observation that in this case the [ν_1 , ν_6] population evolves exactly as in the case of $R(22)$ excitation establishes the dominance of the ν_3 manifold channel [Eq. (23)] as the process filling [ν_1 , ν_6] even in pure CH₂D₂ with either a $R(22)$ or $P(38)$ pump.

An interesting conclusion may be drawn from the comparison of [ν_1 , ν_6] fluorescence signals obtained via the three different pumps. Although the pathway of Eq. (22) results in a faster filling rate of [ν_1 , ν_6] than the pathway of Eq. 23, more population is transferred to [ν_1 , ν_6] via the mechanism of Eq. (23). When only the path illustrated in Eq. 22 is available [$P(24)$ pump], a fast filling rate is observed. When both channels are available for populating [ν_1 , ν_6] [$P(38)$ pump], the rise of [ν_1 , ν_6] is determined by the rate processes of the channel that provides the larger population transfer. In this case, that is the mechanism of Eq. (23). This conclusion was confirmed by numerical modeling of the system.

D. Energy transfer calculations

Processes leading to vibrational equilibration of a multimode system can be divided into two types: near-resonant ladder climbing steps and off-resonant inter-mode exchanges. In CH₂D₂, the processes linking the states at 2000 cm⁻¹ to those at 1000 cm⁻¹ are examples of the first type while the processes that bring about rapid equilibration within the dense manifold at 2000 cm⁻¹ are examples of the second type. The dynamics underlying these two types of processes are not necessarily the same. In near-resonant exchanges of vibrational energy, long range electric multipolar interactions may dominate the dynamics. In such instances, the formulation of Sharma and Brau (S.B.) has been applied with relative success to predict rates of energy exchange.¹³ For large energy gaps, the hard-collisional impact model developed by Schwartz, Slawsky, and Herzfeld has had wide application and some success.¹⁴ The short range forces of the latter model are also operative in near-resonant exchanges in the absence of large electric multipolar moments. This will be shown to be the case in CH₂D₂.

In the S.B. formulation, the interaction potential of colliding partners is expanded in terms of the electric multipole moments of the vibrational transitions involved, with the dipole moment derivative as the leading term. Thus, the dominant term in the expression for the energy transfer probability is the product of the squares of the dipole moments of the vibrational transitions. Therefore, a comparison of this quantity for two systems will yield an estimate of the relative involvement of this mechanism in each system. Such a correlation has been illustrated in Ref. 15. For example, we compare the matrix elements of the first ladder climbing step of the ν_7 mode of CH₂D₂,



to those of a similar process in CH₃F,

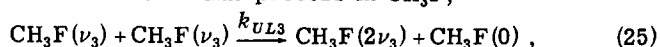


TABLE IV. Near-resonant steps in CH₂D₂.

Process	$\mu_{\nu_x,0}^a$ esu cm × 10 ²⁰	$K_{S.B.}^*$ ^b msec ⁻¹ Torr ⁻¹	K_{SSH}^* ^c msec ⁻¹ Torr ⁻¹
$\nu_1 + \nu_1 \rightarrow 2\nu_1 + 0$	4.46	0.74	342
$\nu_2 + \nu_2 \rightarrow 2\nu_2 + 0$	3.3	0.22	151
$\nu_3 + \nu_3 \rightarrow 2\nu_3 + 0$	3.61	0.32	1440
$\nu_4 + \nu_4 \rightarrow 2\nu_4 + 0$	4.62	0.866	594
$\nu_5 + \nu_5 \rightarrow 2\nu_5 + 0$	d	d	1340
$\nu_6 + \nu_5 \rightarrow 2\nu_6 + 0$	6.09	2.57	310
$\nu_7 + \nu_7 \rightarrow 2\nu_7 + 0$	5.55	1.95	862
$\nu_8 + \nu_8 \rightarrow 2\nu_8 + 0$	4.84	1.02	115
$\nu_9 + \nu_9 \rightarrow 2\nu_9 + 0$	6.2	2.83	1370

^a $\mu_{\nu_x,2\nu_x}$ values are obtained by assuming harmonic oscillator states such that $\mu_{\nu_x,2\nu_x} = 2 \mu_{\nu_x,0}$.

^b $K_{S.B.}^*$ is the upper limit of the rate constant obtained by evaluating the expression of Ref. 15 for exact resonance.

^c K_{SSH}^* is the upper limit of SSH rates calculated by the exact resonance expression given Ref. 20 using $\epsilon/k = 140^\circ\text{K}$, $\rho = 3.82 \text{ \AA}$.

^dNon-IR active mode.

where S.B. calculations predict the observed fast rate constant with relative success (S.B. $\sim 1600 \text{ msec}^{-1} \text{ Torr}^{-1}$, $\text{expt.} \sim 2500 \text{ msec}^{-1} \text{ Torr}^{-1}$)^{10,16}:

$$\frac{k_{UL3}}{k_{UL7}} = \frac{\left(\langle \nu_3 | \frac{\partial \mu}{\partial x} | 0 \rangle^2 \langle \nu_3 | \frac{\partial \mu}{\partial x} | 2\nu_3 \rangle^2 \right)^{\text{CH}_3\text{F}}}{\left(\langle \nu_7 | \frac{\partial \mu}{\partial x} | 0 \rangle^2 \langle \nu_7 | \frac{\partial \mu}{\partial x} | 2\nu_7 \rangle^2 \right)^{\text{CH}_2\text{D}_2}} = \left(\frac{2.17 \times 10^{-19}}{5.55 \times 10^{-20}} \right)^4 = 233. \quad (26)$$

This estimate indicates that the contribution of long range forces to the process of Eq. (24) is over two orders of magnitude smaller than that of the process of Eq. (25). An upper limit for the long range energy transfer cross sections can be obtained by assuming exact resonance, in which case a simple analytical expression can be used to evaluate the rate constants.^{15,17} The results of these calculations together with the dipole moment derivatives for all nine modes of CH₂D₂ are collected in Table IV. The largest rate constant thus obtained is that for the ν_9 mode, which is two orders of magnitude smaller than the experimentally observed rate and of the same order as the $V-T/R$ rate for the molecule. It can therefore be confidently concluded that the involvement of dipolar interactions in the $V-V$ equilibration of CH₂D₂ is minimal. It is also highly unlikely that higher order multiple moments could be of sufficient magnitude to change the conclusion about lack of involvement of long range forces in the $V-V$ equilibration of CH₂D₂.

Calculations of absolute rate constants by the SSH model requires the knowledge of "breathing sphere" parameters of the different vibrational modes. These parameters were computed according to the procedure outlined by Stretton¹⁸ using the normal mode analysis results presented by Deroche.¹⁹ The breathing sphere parameters thus obtained are tabulated (Table V).

Due to the adiabaticity assumptions made in the SSH formulation, SSH calculations best apply to large energy

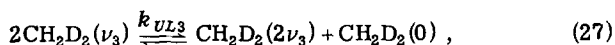
TABLE V. Breathing sphere parameters of CH₂D₂.

Mode	Energy (cm ⁻¹)	$\langle A \rangle^{2*a}$ (amu ⁻¹)
ν_1	2976	0.234
ν_2	2202	0.115
ν_3	1436	0.232
ν_4	1033	0.107
ν_5	1324	0.206
ν_6	3013	0.225
ν_7	1090	0.136
ν_8	2234	0.102
ν_9	1234	0.194

^aIt has been assumed that all angles are the same and equal to those of HCH in CH₄ (109° 28' 16'') and all bond lengths as are assumed equal to those of C-H in CH₄ (1.094 Å) (Ref. 19).

gap processes; however, an analytic solution is possible for the case of exact resonance.²⁰ The expression for exact resonance presented by Tanczos was evaluated for CH₂D₂ by using the Lennard-Jones parameters of CH₄ ($\rho = 3.82$ Å, $\epsilon/R = 140$ °K).²¹ Results are presented in Table IV (k_{SSH}^*). These values are in effect the upper limits of the ladder climbing steps. A comparison of these theoretical values with those available from experiment (ν_3) indicate that the former are somewhat greater than the latter (~2-3 times).

The vibrational levels of CH₂D₂ are not exactly harmonic and therefore the ladder climbing steps are not exactly resonant processes. The calculated SSH probabilities for these processes would be expected to be somewhat reduced from the values calculated for the exactly resonant situation when anharmonicity is taken into account. This correction cannot, however, be conveniently made via direct computation since the SSH formulation breaks down for small energy gaps.²² Thus an interpolation method was used for these calculations. The probability of a process was calculated for hypothetically large energy gaps and a calculation was also performed for a hypothetical exactly resonant case.²⁰ The actual probability of a process was then determined via an interpolation between these values. Thus for a 20 cm⁻¹ anharmonicity, the probability of a transition is reduced ~25% vs the exactly resonant case. This correction is in the correct direction to produce a better agreement between theory and experiment. As an example, for the process

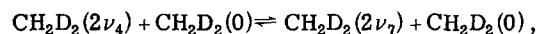
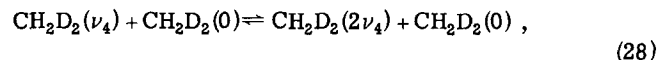


the experimentally determined value for k_{UL3} is 730 ± 80 msec⁻¹ Torr⁻¹, while the SSH value for the case of exact resonance is 1440 msec⁻¹ Torr⁻¹. The corrected SSH value for an energy gap of 20 cm⁻¹ is 1100 msec⁻¹ Torr⁻¹.

The SSH rate constants for all off-resonant intermode exchanges were calculated following the method of Dickens and Ripamonti.²³ The values thus obtained are presented in Table III. Only those rate constants are reported

that have significant values on the V-V timescale (> 1 msec⁻¹ Torr⁻¹).

Calculation of the rates of the equilibration processes within the 2000 cm⁻¹ states of the type



are interesting to consider in that multiple quantum number changes are involved and as such SSH calculations would predict relatively small probabilities for the above equilibration steps.¹⁸ This is contrary to experimental observation. We feel that the observed rapidity of coupling of states in this region is explained by the high density of rovibronic states and their mixing. Such effects are unaccounted for in simple SSH calculations.

Calculated SSH rate constants are, however, in good agreement, on both a relative and absolute basis, with experimental values for near-resonant and off-resonance processes where the states involved are sufficiently removed from each other that their rotational envelopes do not appreciably overlap. Thus, we feel it is justifiable to use SSH calculations to assign the relative efficiencies of V-V processes in CH₂D₂ where this is necessary to partition an overall rate into its constituent rate constants. An example of this is in the parallel mechanism of energy transfer in the lower manifold of CH₂D₂, which is discussed in Sec. IV E. The same concept can be applied for V-T/R rates where more than one state is expected to participate in the deactivation processes.²⁴ Though in V-T/R case absolute rates are not well reproduced by SSH calculations, it seems reasonable to partition the deactivation rate into rate constants by the means of the relative magnitudes of the SSH calculated rate constants. The procedure used is that of Ref. 24 where the overall V-T/R rate of 1 msec⁻¹ Torr⁻¹ is composed of two primary terms:

$$k_{V-T/R} = N_{\nu_4}^0 k_{\nu_4-0} + N_{\nu_7}^0 k_{\nu_7-0},$$

where $N_{\nu_x}^0$ is the fractional equilibrium population of state x and k_{ν_x-0} is the rate constant for the V-T/R deactivation of that state. Relative rates for k_{ν_4-0} and k_{ν_7-0} can be calculated via SSH theory. When this is done the values obtained are $k_{\nu_4-0} = 0.62$ msec⁻¹ Torr⁻¹ and $k_{\nu_7-0} = 0.48$ msec⁻¹ Torr⁻¹. This type of treatment, though perhaps not exact in this case due to the neglect of V-R processes, is necessary in order to obtain specific rate constants for cases where only an overall rate for a process has been deduced from experimental observation. As better calculations appear for the relative magnitude of the deactivation of CH₂D₂ from ν_4 and ν_7 , the values for the actual rate constants can be refined.

In concluding this section, it is interesting to explicitly note the excellent agreement between SSH calculation and observed V-V rates. This is especially interesting in light of the fact that SSH theory was originally formulated to calculate probabilities of processes with large energy gaps. Additionally, CH₂D₂ has a small moment of inertia and, *a priori*, it might be thought that rotational motion would also be an important consideration in the calcula-

tion of V-V rates. Thus, it is indeed possible that this agreement is fortuitous. An interesting test of the ability of SSH calculation to reproduce experimental data would be a study of the temperature dependence of these V-V rate constants and the ability of SSH calculations to reproduce their observed variation as a function of temperature.

E. Numerical modeling

For a system as complex as CH₂D₂, physical intuition cannot be regarded as reliable in discerning rate constants and pathways from observed rates and signal shapes. Similarly, though simplified models of parts of a complex vibrational manifold are often quite useful where applicable, they cannot be expected to accurately reproduce all the behavior observed in a system as complex as CH₂D₂. Thus in order to gain insight into the operative vibrational pathways, to assign rate constants to processes, and finally to verify the mutual consistency of the vibrational pathways proposed in the preceding sections of this paper, a complete numerical model of the CH₂D₂ system was formulated whereby the calculated temporal evolution of the various states in CH₂D₂ could be compared, under a variety of conditions, to the observed temporal evolution of the populations.

This was done by the following procedure. The populations of all states were set equal to their ambient population. The laser pulse was then simulated by depleting the lower state involved in the laser pumping process and adding that population to the upper state of the laser induced transition. Differential equations describing the time evolution of the system were then numerically integrated over experimental timescales. For all initial conditions, convergence of integration and detailed balance were verified. The generated signals (population vs time) were analyzed in a manner identical to the experimental signals. In the course of this work the lower vibrational manifold was modeled separately from the rest of the manifold. This modeling of the lower manifold will be described first and its incorporation into a model for the entire manifold will be considered later in this section.

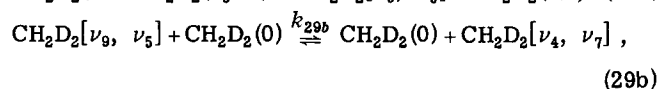
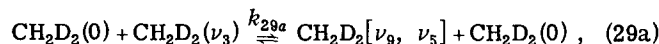
1. Lower manifold model

The experimentally observed signals from the lower manifold are compatible with this part of the manifold behaving as a simple three level system equilibrating via a sequential mechanism. The principal observations that lead to this conclusion are: (1) the signals observed from the ν_9 state are the same with either a ν_4 or ν_7 pump as are the signals from the ν_3 state, (2) there is no apparent induction time on the ν_9 signal but there is an induction time on the ν_3 signal, (3) within experimental error, on a V-V timescale, the signals from ν_9 and ν_3 are composed of only two exponentials.

Clearly, the lower manifold consists of five states and parallel equilibration paths are possible and in some cases are predicted by SSH calculations to be of significant magnitude (see Table III). Therefore, a number of models of the lower manifold were investigated to determine under what circumstances the lower manifold would

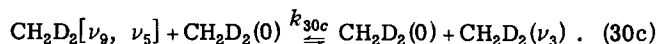
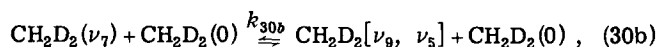
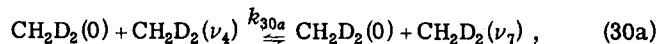
behave in a manner kinetically compatible with the observed signals and therefore also compatible with a three level analysis of the system. It was hoped that numerical modeling of the system coupled with SSH calculations would provide additional insight into the relationship between experimentally determined rates and the actual kinetic rate constants for the operative processes in a full five level model.

In a three level numerical model (I) of the lower manifold, the experimentally observed signals were reproduced with rate constants of 450 and 225 msec⁻¹Torr⁻¹ for the processes illustrated in Eqs. (29a) and (29b), respectively.



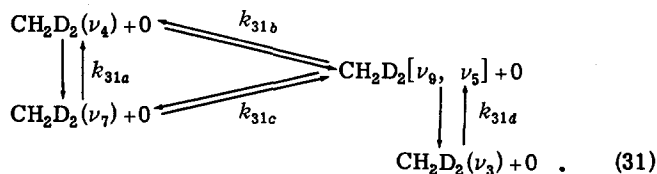
where $[\nu_9, \nu_5]$ and $[\nu_4, \nu_7]$ were taken to be doubly degenerate states at energies of 1267 and 1066 cm⁻¹, respectively.

A four level system (II) consisting of the ν_3 , $[\nu_9, \nu_5]$ and ν_4 and ν_7 states was studied next. A sequential coupling mechanism was considered.



The rate constant for process (30c) was chosen to be the same as that for process (29a). The rate constant for Eq. (30b) was chosen to be equivalent to that of Eq. (29b) and the magnitude of the rate constant for Eq. (30a) was varied to investigate under what conditions this system reproduced the observed rises of the $[\nu_9, \nu_5]$ and ν_3 states following either ν_4 or ν_7 excitation. It was determined that the minimum value of the rate constant k_{30a} necessary to reproduce experimental observation was 600 msec⁻¹Torr⁻¹. The lower limit on the rate constant for 30a varied $\sim \pm 100$ msec⁻¹Torr⁻¹ as the rate constants for processes Eqs. (30b) and (30c) varied over a range compatible with experimental error.

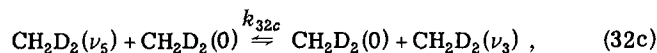
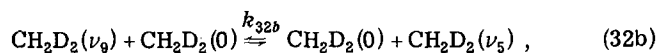
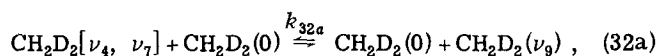
Next a parallel transfer mechanism (III) was considered where the ν_4 and ν_7 states were both coupled to the $[\nu_9, \nu_5]$ state and ν_4 and ν_7 were also coupled to each other as indicated in Eq. (31).



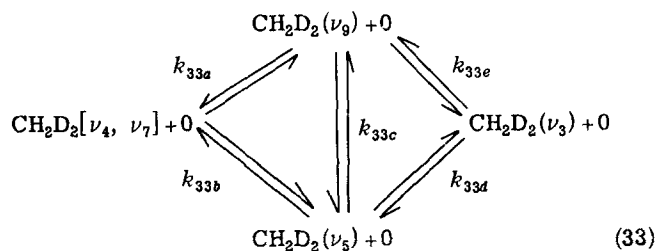
As expected, to produce the observed signal shapes in $[\nu_9, \nu_5]$ and ν_3 and to produce the same rate of rise of $[\nu_9, \nu_5]$ and ν_3 with either a ν_4 or ν_7 pump, the ν_7 to ν_4 rate constant, k_{31a} , must be sufficiently in excess of the rate constants k_{31b} and k_{31c} to provide complete equilibration of ν_4 and ν_7 on the timescale of processes (31b)

and (31c). For k_{31b} and k_{31c} of approximately equal magnitude, it was found that k_{31a} must be $\sim 100 \text{ msec}^{-1} \text{ Torr}^{-1}$ greater than either k_{31b} or k_{31c} to provide for an adequate representation of the experimental system. As the rate constant k_{31c} was increased relative to k_{31b} , it was found that to duplicate experimental signals the magnitude by which k_{31a} had to exceed k_{31c} increased, reaching the sequential mechanism (model II) results asymptotically. Similar results are expected if k_{31b} is increased relative to k_{31c} .

A four level system was then considered where $[\nu_4, \nu_7]$ is considered as a single state and ν_9, ν_5 , and ν_3 were also single states (IV). For a sequential coupling mechanism of the type



The observed signals from ν_9 and ν_3 can be reproduced only if the rate constant for 32b is $\geq 1000 \text{ msec}^{-1} \text{ Torr}^{-1}$. In this situation the signals are best reproduced if the rate constants for the processes of Eqs. (32a) and (32c) have the same values as the respective processes in model I. When parallel paths between $[\nu_4, \nu_7]$ and ν_9 and ν_5 are considered (V)



the situation is somewhat more complicated. In the case where $k_{33a} \cong k_{33b}$, the magnitude of the rate constant k_{33c} is unimportant in establishing equilibrium in the system. Under these circumstances, to reproduce experimental data, k_{33e} and k_{33d} should be each equal to approximately half the magnitude of the rate constant coupling $[\nu_9, \nu_5]$ and ν_3 in the three level model (I), k_{27a} . k_{33a} and k_{33b} each have to be equal to approximately the $[\nu_4, \nu_7] \rightarrow [\nu_9, \nu_5]$ rate constant, k_{29b} , in model (I).

In the case where $k_{33a} \neq k_{33b}$, the magnitude of k_{33c} becomes an important consideration in choosing k_{33e} and k_{33d} . In this situation a variety of combinations of rate constants will adequately reproduce experimental results.

Since there is no reason to believe *a priori* that $k_{33a} = k_{33b}$, some method must be adopted to choose values for the processes in Eq. (33). One reasonable way to do this would be to determine the relative values of k_{33a} and k_{33b} as well as k_{33c} and the pair k_{33e} and k_{33d} via SSH theory.

2. Model for the total vibrational manifold

A numerical model of the vibrational manifold of CH₂D₂ below 3000 cm⁻¹ was investigated. The numerical

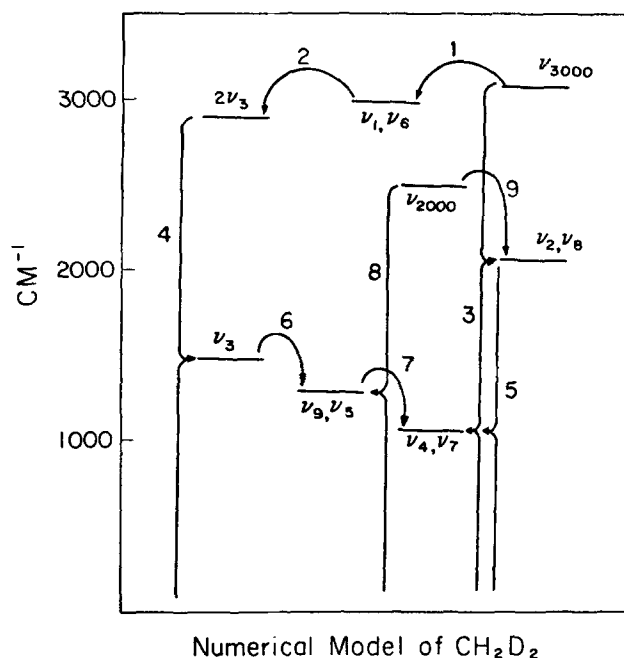


FIG. 7. Numerical model of CH₂D₂. Rates, energies, and degeneracies for processes and states in this model are given in Table VI. Resonant processes are indicated by lines connecting two or more states to the ground state. Nonresonant processes are indicated by an arrow joining two states. Reported rate constants are in the directions indicated by the arrows.

model was based on the sum of the proposed pathways in the system; combining the three level approximation for the lower manifold (I) with the mechanisms proposed for populating the levels in the 2000 cm⁻¹ region and the levels in the 3000 cm⁻¹ region. Figure 7 and Table VI help illustrate this model.

The energies of the fundamentals in the numerical model are those obtained from the spectroscopy of the system. In cases where the coupling among states is rapid or where it is kinetically equivalent to consider multiple states as one multiply degenerate level, this condensation has been performed. The ν_1 and ν_6 fundamentals are combined in this manner as are the ν_2 and ν_8 fundamentals. Rapidly coupled overtone and combination bands (e.g., the 2000 and 3000 cm⁻¹ states) are treated as single multidegenerate states. Since it is not clear how many states should be incorporated into the single multidegenerate state in the 2000 and 3000 cm⁻¹ regions, the energy and degeneracy of these states are considered variables and are varied over a narrow range in an effort to further agreement with experimental data. These combined overtones and combination bands are considered as states separate from the observed fundamentals although under some conditions they may be rapidly coupled to these fundamentals. For example, the $[\nu_1, \nu_6]$ state is coupled through nonresonant processes to the ν_{3000} state, a level representing all the coupled states at 3000 cm⁻¹ and above, that participate in the observed processes. In order to model the behavior of the $[\nu_1, \nu_6]$ state at high pressure of rare gas, the rate from the ν_{3000} state to the $[\nu_1, \nu_6]$ state must be quite large. Although under these circumstances

TABLE VI. Parameters for the numerical model of the full manifold.

State	Energy	Degeneracy	Rates ^a	Process	k (msec ⁻¹ Torr ⁻¹)	Z (collisions) ^b
ν_{3000}	3100	1	1	CH ₂ D ₂ (ν_{3000}) + CH ₂ D ₂ \rightleftharpoons CH ₂ D ₂ ($[\nu_1, \nu_6]$) + CH ₂ D ₂	200	61
$[\nu_1, \nu_6]$	2995	2	2	CH ₂ D ₂ ($[\nu_1, \nu_6]$) + CH ₂ D ₂ \rightleftharpoons CH ₂ D ₂ ($2\nu_3$) + CH ₂ D ₂	450	27
$2\nu_3$	2900	1	3	CH ₂ D ₂ (ν_{3000}) + CH ₂ D ₂ (0) \rightleftharpoons CH ₂ D ₂ ($[\nu_2, \nu_8]$) + CH ₂ D ₂ ($[\nu_4, \nu_7]$)	250	49
ν_{2000}	2400	3	4	CH ₂ D ₂ ($2\nu_3$) + CH ₂ D ₂ (0) \rightleftharpoons 2CH ₂ D ₂ (ν_3)	800	15
$[\nu_2, \nu_8]$	2120	2	5	CH ₂ D ₂ ($[\nu_2, \nu_8]$) + CH ₂ D ₂ (0) \rightleftharpoons 2CH ₂ D ₂ ($[\nu_4, \nu_7]$)	300	41
ν_3	1450	1	6	CH ₂ D ₂ (ν_3) + CH ₂ D ₂ \rightleftharpoons CH ₂ D ₂ ($[\nu_9, \nu_5]$) + CH ₂ D ₂	450	27
$[\nu_9, \nu_5]$	1267	2	7	CH ₂ D ₂ ($[\nu_9, \nu_5]$) + CH ₂ D ₂ \rightleftharpoons CH ₂ D ₂ ($[\nu_4, \nu_7]$) + CH ₂ D ₂	225	55
$[\nu_4, \nu_7]$	1066	2	8	CH ₂ D ₂ (ν_{2000}) + CH ₂ D ₂ (0) \rightleftharpoons 2CH ₂ D ₂ ($[\nu_9, \nu_5]$)	450 ^c	27
			9	CH ₂ D ₂ (ν_{2000}) + CH ₂ D ₂ \rightleftharpoons CH ₂ D ₂ ($[\nu_2, \nu_8]$) + CH ₂ D ₂	5000 ^d	
Laser pumps						
R(22): 1% of the ambient population of the ground state is removed from the ground state and placed in $[\nu_4, \nu_7]$.						
P(38): In addition to the procedure for the R(22) pump simulation, 2.6% of the ambient population of the $[\nu_4, \nu_7]$ state is removed from the $[\nu_4, \nu_7]$ state and added to the ν_{2000} state.						
P(24): 3% of the ambient population of the $[\nu_4, \nu_7]$ state is removed from the $[\nu_4, \nu_7]$ state and added to the ν_{2000} state.						

^aSee Fig. 7. Reverse rates are calculated through detailed balancing.

^bCalculated by the procedure of Ref. 3.

^cUsed to generate the signals in Fig. 2 though its value is arbitrary within the limits discussed in the text.

^dArbitrary as long as > 2000 .

these two levels are rapidly coupled, the actual separation of these states is necessary to reflect the fact that population that flows into the $[\nu_1, \nu_6]$ states from the states in the 2000 cm⁻¹ region must pass through a state or states in the 3000 cm⁻¹ region, approximately 100 cm⁻¹ higher than the $[\nu_1, \nu_6]$ state. This energy gap is reflected in the relative populations of these states and the ratio of the populations is a significant factor in the kinetics linking these states. This kinetic effect has been discussed in great detail in Ref. 7. For the aforementioned reasons, the $2\nu_3$ overtone is also treated as separate from the $[\nu_1, \nu_6]$ state as is the state labeled ν_{2000} , which corresponds to a lumping of states at higher energy than the $[\nu_2, \nu_8]$ state.

By variation of parameters in the model it is required that the 12 observations represented by Fig. 2 be reproduced along with the rare-gas dependence of $[\nu_2, \nu_8]$ and $[\nu_1, \nu_6]$ with an R(22) pump and the rare-gas dependence of the fall of $[\nu_2, \nu_8]$ with a P(38) pump. Though all these observations may not represent linearly independent observables and some may represent observations that have already been used to fix values of variables in the full model, it seems apparent that stringent criteria are being imposed on the model by the number of observations it must simultaneously reproduce.

Whenever possible, rate constants for the full model were chosen from a kinetic analysis of a subset of the system. Thus the rate constants, k_7 and k_8 , were those determined from the three level model analysis. The resonant rate constants (k_3 , k_4 , and k_5) were chosen to be consistent with the rare-gas behavior of the $[\nu_1, \nu_6]$ and $[\nu_2, \nu_8]$ states.⁷ The rate constant k_4 , governing the rate of energy propagation up the ν_3 manifold was chosen to be 800 msec⁻¹ Torr⁻¹ based on its determination in Ref. 7 as 730 ± 70 msec⁻¹ Torr⁻¹. As previously stated, the assignment of a value to this rate constant was based on the leveling behavior of $[\nu_1, \nu_6]$ in the region of high

rare-gas pressure. In this region the major source of filling of $[\nu_1, \nu_6]$ is via the ν_3 manifold. In this high pressure region, the observed leveling rate of $[\nu_1, \nu_6]$ is dependent on the rate of the resonant step up the ν_3 manifold, the populations of the states involved in the filling of $[\nu_1, \nu_6]$, and the rate for the other filling pathway, via the states in the 2000 cm⁻¹ region. Since the rise rate of the states in the 2000 cm⁻¹ region is rare-gas pressure independent, its maximum contribution to the filling of $[\nu_1, \nu_6]$ can be accounted for, yielding a determination for the value of k_4 that is largely model independent. Having determined a value for k_4 , the value for k_2 is fixed and can be determined by the intercept of the rare-gas dependent curve (Fig. 4) for the rise rate of $[\nu_1, \nu_6]$ as discussed in Ref. 7. A similar determination could, in theory, be made for the rate constants k_3 and k_5 if not for the fact that there is evidence to be presented later in this section that the addition of rare gas may open up new channels for populating the 2000 cm⁻¹ states. Addition of rare gas would be expected to equilibrate the lower manifold more rapidly, increasing the proportion of population that is excited to the 2000 cm⁻¹ region through the $[\nu_9, \nu_5]$ resonant channel and decreasing the proportion excited through the resonant $[\nu_4, \nu_7]$ channel. Though this behavior is mandated by and can be easily fit to the experimental data, because of this effect unique rate constants cannot be determined for transfer up the $[\nu_4, \nu_7]$ manifold.

The $[\nu_2, \nu_8]$ to $[\nu_4, \nu_7]$ rate constant, k_5 , was varied until the $[\nu_2, \nu_8]$ rise rate agreed with the experimental rise rate in the 2000 cm⁻¹ region for R(22) laser line excitation. The ν_{3000} to ν_{2000} rate constant, k_3 , was varied to fit the observed rise of $[\nu_1, \nu_6]$ with P(24) hot band excitation. A finite value for k_8 is necessary to reproduce the rare-gas dependent behavior of $[\nu_2, \nu_8]$ but its magnitude can be chosen rather arbitrarily since neither the rate of rise of the $[\nu_2, \nu_8]$ nor that of the $[\nu_9,$

ν_5] state is significantly dependent on its magnitude. The ν_{3000} to $[\nu_1, \nu_6]$ rate constant, k_1 , can be chosen over a fairly wide range of values as these states contain little population and therefore act as a small perturbation on the $[\nu_1, \nu_6]$ state. The $[\nu_2, \nu_8] \rightarrow \nu_{2000}$ rate constant, k_7 , was chosen to be of sufficient magnitude that transfer between these states is instantaneous on the timescale of the experiment.

With the preceding as input data, the following differential equations were integrated under three sets of initial conditions.

$$\frac{dN_{\nu_{3000}}}{N_g dt} = -N_{\nu_{3000}}(k_1 + k_3) + k_{-1}N_{[\nu_1, \nu_6]} + \frac{k_{-3}N_{[\nu_2, \nu_8]}N_{[\nu_4, \nu_7]}}{N_g},$$

$$\frac{dN_{[\nu_1, \nu_6]}}{N_g dt} = -N_{[\nu_1, \nu_6]}(k_{-1} + k_2) + k_1N_{\nu_{3000}} + k_{-2}N_{2\nu_3},$$

$$\frac{dN_{2\nu_3}}{N_g dt} = -N_{2\nu_3}(k_{-2} + k_4) + k_2N_{[\nu_1, \nu_6]} + k_{-4}N_{\nu_3}^2/N_g,$$

$$\frac{dN_{\nu_{2000}}}{N_g dt} = -N_{\nu_{2000}}(k_9 + k_8) + k_{-9}N_{[\nu_2, \nu_8]} + k_{-8}N_{[\nu_9, \nu_5]}^2/N_g,$$

$$\begin{aligned} \frac{dN_{[\nu_2, \nu_8]}}{N_g dt} = & -N_{[\nu_2, \nu_8]} \left(k_{-9} + \frac{k_{-3}N_{[\nu_4, \nu_7]}}{N_g} + k_5 \right) + k_9N_{\nu_{2000}} \\ & + k_3N_{\nu_{3000}} + k_{-5}N_{[\nu_4, \nu_7]}^2/N_g, \end{aligned}$$

$$\frac{dN_{\nu_3}}{N_g dt} = -N_{\nu_3} \left(k_6 + \frac{2k_{-4}N_{\nu_3}}{N_g} \right) + 2k_4N_{2\nu_3}N_g + k_{-6}N_{[\nu_9, \nu_5]},$$

$$\begin{aligned} \frac{dN_{[\nu_9, \nu_5]}}{N_g dt} = & -N_{[\nu_9, \nu_5]} \left(k_{-6} + k_7 + 2k_{-8} \frac{N_{[\nu_9, \nu_5]}}{N_g} \right) + k_6N_{\nu_3} \\ & + k_{-7}N_{[\nu_4, \nu_7]} + 2k_8N_{\nu_{2000}}, \end{aligned}$$

$$\begin{aligned} \frac{dN_{[\nu_4, \nu_7]}}{N_g dt} = & -N_{[\nu_4, \nu_7]} \left(k_{-7} + 2k_{-5} \frac{N_{[\nu_4, \nu_7]}}{N_g} + k_{-3} \frac{N_{[\nu_2, \nu_8]}}{N_g} \right) \\ & + 2k_5N_{[\nu_2, \nu_8]} + k_3N_{\nu_{3000}} + k_7N_{[\nu_9, \nu_5]}, \end{aligned}$$

$$\begin{aligned} \frac{dN_g}{N_g dt} = & -(k_3N_{\nu_{3000}} + k_4N_{2\nu_3} + k_5N_{[\nu_2, \nu_8]} + k_8N_{\nu_{2000}}) \\ & + (k_{-3}N_{[\nu_4, \nu_7]}N_{[\nu_2, \nu_8]} + k_{-4}N_{\nu_3}^2 \\ & + k_{-5}N_{[\nu_4, \nu_7]}^2 + k_{-6}N_{[\nu_9, \nu_5]}^2)/N_g, \end{aligned}$$

where rate constants with negative subscripts are in the direction opposite to those indicated in Fig. 7 and N_g represent the ground state. For each set of initial conditions a percentage of the ambient Boltzmann population in the initial state of the transition induced by the laser was transferred into the final state of the transition and the differential equations were integrated starting at that point.

For the first set of initial conditions, intended to simulate excitation of the $[\nu_4, \nu_7]$ state with the $R(22)$ line of the laser, 1%–5% of the ambient population of the ground state was transferred into the $[\nu_4, \nu_7]$ level. It was found that the rates obtained from the experimental signals did not change over the range of initial population transfer used.

To simulate the hot band transition induced by the $P(24)$ line a percentage of the population of the $[\nu_4, \nu_7]$ state was transferred to the $[\nu_2, \nu_8]$ state. The appropriate percentage to be transferred was unknown. It was found that for given degeneracies in the 3000 and 2000 cm^{-1}

states the percentage of the original amplitude to which the $[\nu_1, \nu_6]$ decayed (Fig. 2) was inversely proportional to the percentage of the population initially transferred out of the $[\nu_4, \nu_7]$ mode and into the $[\nu_2, \nu_8]$ mode. The value given in Table VI was chosen to provide a reasonable fit to the $[\nu_1, \nu_6]$ decay. However, varying the degeneracies of states in the 2000 and 3000 cm^{-1} region varied this percentage proportionately.

The third set of initial conditions corresponded to excitation using the $P(38)$ laser line inducing both ground state to $[\nu_4, \nu_7]$ and $[\nu_4, \nu_7]$ to $[\nu_2, \nu_8]$ transitions. This was obtained by simultaneously transferring population from the ground state to the $[\nu_4, \nu_7]$ mode and from the $[\nu_4, \nu_7]$ mode to the $[\nu_2, \nu_8]$ state and commencing integration from there. The relative percentage for each transfer was obtained in a manner similar to that used with the $P(24)$ line. The amplitude to which the $[\nu_2, \nu_8]$ decayed with the $P(38)$ line was used as an indicator of the ratio of the populations involved in the two transfers. These percentages were varied until the numerically generated signal matched the experimental signal.

The model, if accepted, allows us to infer at least one additional feature regarding vibrational energy transfer in CH₂D₂. This is the necessity of the transfer of energy from the $[\nu_9, \nu_5]$ mode to the $[\nu_2, \nu_8]$ mode, a conclusion arrived at in the following manner. The rise rate of the $[\nu_2, \nu_8]$ mode was observed while increasing the rate between the $[\nu_9, \nu_5]$ and $[\nu_4, \nu_7]$ states. It was found that increasing the rate of energy transfer between the $[\nu_9, \nu_5]$ and $[\nu_4, \nu_7]$ had little effect upon the $[\nu_2, \nu_8]$ rise rate only if the $[\nu_9, \nu_5]$ state was coupled to the $[\nu_2, \nu_8]$ state. This behavior is consistent with the experimental situation in which rare gas accelerated the nonresonant $[\nu_9, \nu_5]$ to $[\nu_4, \nu_7]$ transition and no significant increase in the rise rate of the $[\nu_2, \nu_8]$ state is observed. (Rare gas would also accelerate the ν_3 to $[\nu_9, \nu_5]$ transition but this was seen to have little effect upon the $[\nu_2, \nu_8]$ rise rate in the model.) If no coupling was provided between the $[\nu_9, \nu_5]$ and $[\nu_2, \nu_8]$ states, increasing the $[\nu_9, \nu_5]$ to $[\nu_4, \nu_7]$ rate resulted in a significant decrease in the $[\nu_2, \nu_8]$ rise rate, a result clearly inconsistent with experiment. Therefore it is felt that resonant transfer occurs not only from the $[\nu_4, \nu_7]$ state to the $[\nu_2, \nu_8]$ state, but from the $[\nu_9, \nu_5]$ to the $[\nu_2, \nu_8]$ state. This coupling is expected to be through an intermediate state, an overtone or combination band, in the 2000 cm^{-1} region [see Eq. (21a)]. However, the rate of rise of $[\nu_2, \nu_8]$ is mostly determined by the $[\nu_4, \nu_7]$ channel. This can be understood by the fact that both $[\nu_9, \nu_5]$ and the corresponding overtones have significantly less population than the corresponding states for the $[\nu_4, \nu_7]$ channel.

V. CONCLUSIONS

By the use of a variety of complementary laser induced fluorescence techniques a great deal of highly specific information has been gained regarding vibrational equilibration pathways and rates in the CH₂D₂ molecule. Multiple laser pumps have allowed for probing of how the molecule responds to perturbations corresponding to different initial conditions for $V-V$ equilibration. The rare-gas dependence of $V-V$ processes involved in the rise and fall of different states has been a great aid in

pinpointing the role of resonant $V-V$ processes involving the collision of two excited molecules in a given equilibration step. It has also allowed for facile discrimination between these types of processes and the involvement of nonresonant $V-V$ channels in an equilibration step. An "impurity" molecule, O₂, has been used as a probe of a specific equilibration step in CH₂D₂. By determining the amount of vibrational energy that flows from the CH₂D₂ manifold to O₂ upon their equilibration, it is possible to rule out a variety of pathways for equilibration processes coupling the ν_3 mode with other states in CH₂D₂. These studies coupled with a variety of other observations leads to a unique determination of the filling pathway for the ν_3 mode.

A numerical model of the CH₂D₂ vibrational manifold was formulated as an aid in evaluating the proposed $V-V$ equilibration pathways. The final numerical model of the system provides an excellent reproduction of experimental signals. This is illustrated in Fig. 2 and in Table VI where the input parameters for the model are reported. The numerical model has provided a number of additional insight into $V-V$ processes in CH₂D₂.

Both SSH and Sharma and Brau type energy transfer calculations have been performed on the system. These calculations indicate that, due to the small dipole moment derivatives of CH₂D₂ fundamentals, the dynamics of energy transfer in this system are probably controlled by the repulsive part of the intermolecular potential. Interestingly, where comparisons can reasonably be made, SSH calculations for $V-V$ steps in the system come very close to predicting experimentally determined rates and rate constants.

The combined results of the above studies have led to a quite specific determination of operative $V-V$ pathways in this system. The lower states (ν_3 , ν_9 , ν_5 , ν_4 , ν_7) in the vibrational manifold behave kinetically like a three level system. The pairs of levels, [ν_4 , ν_7] and [ν_9 , ν_5] are expected to be coupled rapidly due to proximity and rotational overlap. Therefore the major equilibration processes in the lower manifold can probably be described as sequential processes, as illustrated in Eq. (17). Under these circumstances rate constants can be determined for these processes and are reported. However, if the coupling between ν_4 and ν_7 in one case and ν_9 and ν_5 in the other is not sufficiently rapid to make these states appear to behave kinetically as a single state, then to determine specific rate constants, the exact magnitude of the processes coupling ν_4 and ν_7 and ν_9 and ν_5 must be considered along with the exact magnitude of possible parallel equilibration pathways, such as those in Eq. (3). Under these conditions, enough experimental data does not exist to uniquely determine all the rate constants necessary to characterize equilibration of the lower manifold. Reasonable estimates of the rate constants, however, can be made by the additional consideration of the relative magnitudes of SSH calculated rate constants for the $V-V$ processes in the lower manifold. Interestingly, the rate constants for the three level model of the lower manifold in CH₂D₂ are quite similar to the rate constants for the analogous processes in the lower manifold of CH₃F.¹⁰ Evidence is

presented to indicate that direct coupling between [ν_4 , ν_7] and ν_3 is negligible and that direct population transfer between ν_3 and the states in the 2000 cm⁻¹ region is negligible.

The ν_2 and ν_8 states appear to be rapidly coupled, not only to each other but also to most if not all of the overtones and combination bands in the 2000 cm⁻¹ region. The mechanism responsible for populating these states involves resonant transfer from states in the 1000 cm⁻¹ region. The majority of the population transferred to the 2000 cm⁻¹ region comes from the ν_4 and ν_7 states. However, the full numerical model indicates that some of the population in the 2000 cm⁻¹ region must also come from the ν_9 and ν_5 states if the rare-gas dependence of the 2000 cm⁻¹ states in the numerical model is to be compatible with the experimentally observed rare-gas dependence for these states.

The ν_1 and ν_6 states also appear to be rapidly coupled. With an $R(22)$ or $P(38)$ pump they are simultaneously filled by two pathways: one involves resonant sequential transfers from the states in the 1000 cm⁻¹ region to states in the 2000 cm⁻¹ region to states in the 3000 cm⁻¹ region and then finally a nonresonant step to the [ν_1 , ν_8] state. The other involves an initial nonresonant transfer from the pumped state to ν_3 and then transfer from ν_3 to $2\nu_3$ and crossover to [ν_1 , ν_6]. It is found that the pathway up the ν_3 manifold is dominant.

Finally this detailed determination of vibrational pathways has allowed for the unique determination of a number of rate constants for the system.

ACKNOWLEDGMENTS

We gratefully acknowledge support by the donors of the Petroleum Research Fund administered by the American Chemical Society and the National Science Foundation under grants CHE 76-10333 and CHE 79-08501.

- ¹(a) E. Weitz and G. W. Flynn, *Adv. Chem. Phys.* (to be published); (b) B. L. Earl, L. A. Gamss, and A. M. Ronn, *Acc. Chem. Res.* **11**, 183 (1978); (c) C. B. Moore, *Adv. Chem. Phys.* **23**, 41 (1973); (d) E. Weitz and G. W. Flynn, *Annu. Rev. Phys. Chem.* **25**, 275 (1974).
- ²(a) M. Morillon-Chapey and C. Alamichel, *Can. J. Phys.* **51**, 2189 (1973); (b) J. C. Deroche, *J. Phys.* **34**, 559 (1973); (c) J. C. Deroche and G. Guelachvili, *J. Mol. Spectrosc.* **56**, 76 (1975); (d) J. C. Deroche, G. Graner, and A. Cabane, *ibid.* **57**, 331 (1975); (e) J. C. Deroche and P. Pinson, *ibid.* **58**, 229 (1975).
- ³V. A. Apkarian and E. Weitz, *Chem. Phys. Lett.* **59**, 414 (1978).
- ⁴(a) D. S. Y. Hsu and T. J. Manuccia, *Appl. Phys. Lett.* **33**, 9151 (1978); (b) **36**(8), 714 (1980).
- ⁵J. Finzi and C. B. Moore, *J. Chem. Phys.* **63**, 2285 (1975).
- ⁶K. H. Casleton and G. W. Flynn, *J. Chem. Phys.* **67**, 3133 (1977).
- ⁷V. A. Apkarian and E. Weitz, *J. Chem. Phys.* **71**, 4349 (1979).
- ⁸J. M. Preses, G. W. Flynn, and E. Weitz, *J. Chem. Phys.* **69**, 2782 (1978).
- ⁹G. T. Fujimoto and E. Weitz, *J. Chem. Phys.* **27**, 65 (1978).
- ¹⁰R. S. Sheory and G. W. Flynn, *J. Chem. Phys.* **72**, 1175 (1980).
- ¹¹T. M. Lowry and W. T. John, *J. Chem. Soc. London* **97**,

- 2634 (1910).
- ¹²L. M. Sverdlov, *Opt. Spektrosk.* **10**, 33 (1961).
- ¹³R. D. Sharma and C. A. Brau, *J. Chem. Phys.* **50**, 924 (1969).
- ¹⁴R. N. Schwartz, Z. I. Slawsky, and K. F. Herzfeld, *J. Chem. Phys.* **20**, 1591 (1952).
- ¹⁵J. C. Stephenson and C. B. Moore, *J. Chem. Phys.* **52**, 2333 (1970).
- ¹⁶J. M. Preses and G. W. Flynn, *J. Chem. Phys.* **66**, 3112 (1977).
- ¹⁷B. H. Mahan, *J. Chem. Phys.* **46**, 98 (1967).
- ¹⁸J. L. Stretton, *Trans. Faraday Soc.* **61**, 1053 (1965).
- ¹⁹J. C. Deroche, Ph.D. thesis, Université de Paris-Sud, Orsay, 1977.
- ²⁰P. I. Tanczos, *J. Chem. Phys.* **25**, 439 (1956).
- ²¹J. O. Hirschfelder, C. F. Curtiss, and R. B. Bird, *Molecular Theory of Gases and Liquids* (Wiley, New York, 1964).
- ²²K. F. Herzfeld and T. A. Litovitz, *Absorption and Dispersion of Ultrasonic Waves* (Academic, New York, 1959).
- ²³P. G. Dickens and A. Ripamonti, *Trans. Faraday Soc.* **57**, 735 (1961).
- ²⁴E. Weitz and G. W. Flynn, *J. Chem. Phys.* **58**, 2679 (1973).